www.sciencemag.org/cgi/content/full/science.1208144/DC1

Supporting Online Material for

Stochastic Pulse Regulation in Bacterial Stress Response

James C. W. Locke,* Jonathan W. Young,* Michelle Fontes,
María Jesús Hernández Jiménez, Michael B. Elowitz

*To whom correspondence should be addressed. E-mail: melowitz@caltech.edu

Published 6 October 2011 on *Science* Express
DOI: 10.1126/science.1208144

This PDF file includes:

Other Supporting Online Material for this manuscript includes the following:
(available at www.sciencemag.org/cgi/content/full/science.1208144/DC1)

Stochastic Pulse Regulation in Bacterial Stress Response

Supplementary Information

Plasmid construction

All plasmids were cloned using *E.coli* strain Dh5α and a combination of standard molecular cloning techniques and non-ligase dependent cloning using Clontech In-Fusion Advantage PCR Cloning kits. Plasmid constructs were integrated into *B. subtilis* chromosomal regions via double crossover using standard techniques. The following list provides a description of each plasmid constructed, with details on integration position/cassette and selection marker given at the beginning. Note that all plasmids below replicate in *E. coli* but not in *B. subtilis*.

Plasmid list:

1) *ppsb::P_{trpE}-mCherry Erm^R* - This plasmid was used to provide uniform expression of mCherry from a σ^A-dependent promoter, enabling automatic image segmentation (cell identification) in time-lapse movie analysis. A minimal σ^A promoter was used from the *trpE* gene and cloned into a vector with *ppsb* homology regions. The original integration vector was a gift from A. Eldar [1]. For some strains, the selection marker was subsequently changed, in *B. subtilis,* to either *Kan^R* or *Phleo^R.*
2) *sacA::P_{sigB}-yfp Cm^R* - The promoter immediately upstream of RsbV, containing a well-characterized σ^B promoter, was cloned into the EcoRI/BamHI sites of AEC127 [1], yielding a Venus (YFP) reporter for σ^B activity.
3) *amyE::$P_{hyperspank}$-X Spect^R* - Where X = *rsbW, rsbV, rsbQP, rsbVW, rsbVWB, yfp*. The coding region of each single gene or combination, along with a 5' transcriptional terminator, was cloned behind the $P_{hyperspank}$ IPTG-inducible promoter in plasmid pDR-111 (gift of D. Rudner, Harvard).
4) *amyE*::*P_{spac}-Y Spect^R* - Where Y = *rsbQP-yfp, rsbTU-yfp, yfp*. The P_{spac} promoter is also controlled by IPTG, but promoter leakiness (basal expression) is less than $P_{hyperspank}$ (D. Rudner, Harvard). This reduced leakiness allowed modulation of low levels of phosphatase.
5) *amyE::P_{sweet}-TU Spect^R.* The *rsbTU* coding region was cloned into pdr160 (gift of D. Rudner, Harvard). P_{sweet} is induced by xylose. Although full activation is not achieved in the presence of glucose, the absence of maximal expression did not adversely affect results under our conditions.
6) *amyE::P_{sweet}-yfp Spect^R.* Originally pdr160 (a kind gift of D. Rudner). The *yfp* gene was cloned into this plasmid in order to compare expression levels between the different inducible promoters.
7) *amyE:: 3xCFP Spect^R.* We constructed an integration plasmid based on pDL30 in which 3 separate copies of *cfp*, each with its own RBS were constructed with a multiple cloning site preceding the first *cfp*.
8) *amyE::P_{sigb}-3xCFP Spect^R.* This alternative σ^B reporter, containing three tandem copies of the CFP fluorescent protein gene, was used in combination with *yfp* reporters of different genes.

9) *sacA::cfp* Cm^R - An integration vector where *cfp* replaced the *yfp* gene from AEC127.
10) *sacA::* P_{sigb} *-cfp* Cm^R - The same upstream promoter of RsbV (as in plasmid (2) above) was cloned into plasmid (9), providing a CFP reporter for σ^B activity integrated in the *sacA* locus.
11) *amyE::*P_{QP}*-QP-yfp* $Spect^R$ - A derivative of the original plasmid (3), where $P_{hyperspank}$ was removed and replaced with the *QP* gene along with the upstream coding region of this operon.
12) *sacA::X-yfp* Cm^R - *Where X =* P_{yfla}, P_{csbB}, P_{cmp}, P_{ctc}, P_{gsib}, P_{gspA}. The promoters immediately upstream of various target genes of σ^B, were cloned into the EcoRI/BamHI sites of AEC127 [1], yielding Venus (YFP) reporters for each of these downstream targets of σ^B.
13) *thrC::* P_{sweet}*-RsbW* Erm^R- We constructed an integration plasmid where the xylose repressor and the promoter responsive to xylR (P_{sweet}) from pdr160 (see above) was subcloned into pDG1664 (or ECE117 from the Bacillus Genomic Stock Center (BGSC)). The gene *RsbW* was then subcloned into this plasmid.

B. subtilis strains

Strains used were in the PB2 genetic background, except where noted. Antibiotic resistance was switched using a previously described antibiotic switching vector system [2]. Deletions were made by replacing genes of interest with a selection marker via a linear DNA fragment homologus to the region of interest. Many starting strains/genomic DNA were kind gifts of C.W. Price (see references below). Under construction procedure, the '→' symbol indicates an integration event from plasmid or genomic DNA into the strain after the arrow. For example, in strain JJB730, the construction procedure is listed as "*JJB461 (selection on Tet)→JJB635 (selection on Erm)→JJB176*," meaning, "the genomic DNA of JJB635 was prepared and transformed into JJB176 with selection on Erm; This strain was then transformed with the genomic DNA of JJB461, with selection on Tet."

Table S1: Strain information and construction

#	Strain name	Genotype	Construction Procedure	Used in figure	Reference
1	PB2	*trpC2 (this genotype omitted in derived strains, below)*			BGSC 1A776
2	JJB174	PB2; *ppsb::*P_{trpE}-mCh *neo*^{R}	Plasmid (1) above → PY79 → PB2. Antibiotic cassette switched from Erm^R to Neo^R		This work
3	JJB176	PB2; *ppsb::*P_{trpE}*-mCh Phleo*^{R}	Plasmid (1) above → PY79 → PB2. Antibiotic cassette switched from Erm^R to $Phleo^R$	Negative control for snapshots	This work
4	JJB213	JJB176; *sacA::*P_{sigB}*-yfp* Cm^R	Plasmid (2) above → JJB176		
5	JJB240	JJB174; *delRsbU; sacA::* P_{sigB}*-yfp* Cm^R	Plasmid (2) above →JJB174 →PB494 [3]	1C-F, S(1-4), S6	This work and [3]
6	JJB256	JJB213; *sigB::* $Spect^R$	BGSC 1A780 → JJB213		This work
7	JJB332	JJB240; *amyE::*$P_{hyperspank}$*-rsbV* $Spect^R$	Plasmid (3, RsbV) above → JJB240	S9	This work
8	JJB334	JJB240; *amyE::*$P_{hyperspank}$*-rsbW* $Spect^R$	Plasmid (3, RsbW) above → JJB240	S9	This work
9	JJB367	JJB240; *amyE::*P_{sigB}-3X*cfp* $Spect^R$	Plasmid(8) → JJB240		This work
10	JJB413	JJB240; *amyE::*$P_{hyperspank}$*-rsbQP* $Spect^R$	Plasmid (3, RsbQP) above → JJB240	S9	This work
11	JJB415	JJB240; *amyE::*$P_{hyperspank}$*-rsbVW* $Spect^R$	Plasmid (3, RsbVW) above → JJB240	S9	This work

12	JJB423	JJB240; *amyE::*$P_{hyperspank}$-*rsbVWB* $Spect^R$	Plasmid (3, RsbVWB) above → JJB240	S9	This work
13	JJB432	JJB176; *amyE::*$P_{hyperspank}$-*yfp* $Spect^R$	Plasmid (3, yfp) above → JJB176	S9 (induction level)	This work
14	JJB434	JJB176; *amyE::*P_{spac}-*yfp spect*^{R}	Plasmid (4, yfp) above → JJB176		This work
15	JJB461	JJB240; *rsbQP::*Tet^R	Δ*rsbQP* Tet^R recombination at the *rsbQP* locus → JJB240	S2	This work
16	JJB467	JJB461; *rsbU::*Tet^R; P_{spac}-*rsbVWBX* Erm^R	JJB469 → JJB461 (with Erm^R selection)		This work
17	JJB469	JJB176; *rsbU::*Tet^R; P_{spac}-*rsbVWBX* Erm^R	Δ*rsbU* Tet^R recombination at the RsbU locus → PB212 [4] → JJB176		This work and [4]
18	JJB503	JJB176; *amyE::* P_{sweet}-*yfp* $Spect^R$	Plasmid(6) above → JJB176		This work
19	JJB578	JJB467; *amyE::* P_{sweet}-TU $Spect^R$	Plasmid(6) above → JJB467	3B, S14, S18	This work
20	JJB556	JJB367; *sacA::*P_{yflA}-*yfp* Cm^R	Plasmid(12,P_{yflA}-yfp) → JJB367	S5	This work
21	JJB559	JJB367; *sacA::*P_{csbB}-*yfp* Cm^R	Plasmid(12,P_{csbB}- yfp) → JJB367	S5	This work
22	JJB564	JJB367; *sacA::*P_{ctC}-*yfp* Cm^R	Plasmid(12,P_{ctc}- yfp) → JJB367	S5	This work
23	JJB563	JJB367; *sacA::*P_{qsiB}-*yfp* Cm^R	Plasmid(12,P_{qsiB}- yfp) → JJB367	S5	This work
24	JJB565	JJB367; *sacA::*P_{qspA}-*yfp* Cm^R	Plasmid(12,P_{qspA}- yfp) → JJB367	S5	This work
25	JJB567	JJB367; sacA:: P_{cmp}-*yfp* Cm^R	Plasmid(12,P_{cmp}- yfp) → JJB367	S5	This work
26	JJB572	JJB367; *sacA::*P_{sigB}-*yfp* Cm^R	Plasmid(12,P_{sigB}- yfp) → JJB367	S5	This work
27	JJB629	JJB213; *rsbQP::*Tet^R	JJB461 → JJB213 (with Tet^R selection)	S2	This work
28	JJB635	JJB176; *RsbR-U::*Erm^R	*ΔrsbRU* Erm^R recombination at the *rsbRU* locus		This work
29	JJB637	JJB635; *rsbQP::*Tet^R	JJB461 → JJB635 (with Tet^R selection)		This work
30	JJB643	JJB637; *amyE::* P_{spac}-*rsbTU* $Spect^R$	Plasmid (4, RsbTU) above → JJB637	4D, S17, S18, S20	This work
31	JJB675	PY79; *amyE::* P_{spank}-ftsW $Spect^R$; *ftsW::Tet*^{R} *; ppsb*::P_{trpe}-mCh Neo^R	JJB174→ sub-strain of Fili-SOG from Suel [5]		This work and [5]
32	JJB676	JJB675; *sacA::*P_{sigB}-*yfp* Cm^R	Plasmid (2) above → JJB675		This work
33	JJB712	JJB676; *rsbR-U::*Erm^R	JJB635(selection on Erm) →JJB676	2A-B, S7, S8	This work
34	JJB730	JJB176; *rsbR-U::*Erm^R; *rsbQP::*Tet^R	JJB461 (selection on Tet) →JJB635 (selection on Erm) → JJB176		This work
35	JJB733	JJB730; *sacA::*P_{sigB}-*cfp* Cm^R	Plasmid(10) above → JJB730		This work
36	JJB736	JJB733; *amyE::* P_{spac}-*rsbTU-yfp* $Spect^R$	Plasmid(4,TU-yfp) → JJB733	S11	This work
37	JJB737	JJB733; *amyE::* P_{spac}-*rsbQP-yfp* $Spect^R$	Plasmid(4,QP-yfp) → JJB733	2C, S11	This work
38	JJB739	JJB733;*amyE::*P_{rsbQP}-*rsbQP-yfp* $Spect^R$	Plasmid(11) → JJB733	S15, S16	This work
39	JJB746	JJB710; *rsbQP::*$Tet^{R;}$; *sacA::*P_{sigB}-*cfp* Cm^R	JJB461 (selection on Tet) → Plasmid(10) above → JJB176		This work
40	JJB749	JJB746; P_{sweet}-*rsbTU-yfp* $Spect^R$; RsbU:: Tet^R; P_{spac}-*rsbVWBX* Erm^R	Plasmid(4,TU-yfp) → JJB469 (selection on Erm) →JJB746	S12	This work
41	JJB780	JJB174; P_{spac}-*rsbQP-yfp; sacA::* P_{sigB}-*cfp* Cm^R*; delRsbU;*	Plasmid(4,QP-yfp) →*sacA::* P_{sigB}-*cfp* Cm^R →JJB176→PB494 [3]		This work and [3]
42	JJB781	JJB176; *sacA::*P_{sigB}-*cfp* Cm^R; *rsbR-U::*Erm^R	JJB635(selection on Erm) →Plasmid(10)→JJB176	S15	This work
43	JJB819	JJB780; P_{sweet}-*rsbW* Erm^R; *rsbQP::*$Tet^{R;}$	JJB461 (selection on Tet) →plasmid(13)→JJB780	S13	This work

Microscopy

All data were acquired using a CoolSnap HQ2 attached to a Nikon inverted TI-E microscope, equipped with the Nikon Perfect Focus System (PFS) hardware autofocus module. Molecular Devices commercial software (Metamorph 7.5.6.0) controlled microscope, camera, motorized stage (ASI instruments), and epifluorescent and brightfield shutters (Sutter Instruments). Epi-illumination was provided by a 300 W Xenon light source (LamdbaLS, Sutter instruments) connected via a liquid light guide into the illuminator of the scope. Phase contrast illumination was provided by a halogen bulb to allow verification of cell focus and cell shape. Temperature control was achieved using an enclosed microscope chamber (Nikon) attached to a temperature sensitive heat exchanger set to 37C. All experiments used a Phase 100x Plan Apo (NA 1.4) objective, except for experiments involving filamentous cells, which used a 60x Plan Apo (NA 1.4) objective. Chroma filter sets used were as follows: #41027 (mCh), #41028 (YFP), and #31044v2 (CFP).

Sample Preparation

Between days, relative lamp intensity levels were monitored by taking an image of fluorescent beads and measuring their mean intensity. Exposure times were then adjusted to keep per exposure light levels constant between experiments. For snapshots, cells were spotted on 1.5% low melt agarose in PBS and imaged. Images were then analyzed via custom Matlab software, where mean cell intensities were background corrected using strain JJB176, which has mCherry expression for segmentation, but lacks YFP or CFP expression. For most time-lapse movies (unless otherwise specified), larger 1.5% low melt agarose pads were prepared by pipetting 1 mL of media/agarose solution and allowed to solidify between two 22 x 22mm coverglass (no. 1). A 6 mm biopsy punch cut the larger pad into smaller uniform sized pads, to which 2.25 μL of culture diluted to OD 0.01 was pipetted. This protocol tended to give consistent and well-separated densities on the pad, ideal for time-lapse conditions. Prepared pads were then enclosed in coverglass bottom dishes (Willco #HBSt-5040) and sealed with parafilm or grease to prevent evaporation.

Growth Conditions

Media

SMM is derived from Spizizen's minimal media [6], which uses 0.5% glucose as the carbon source and tryptophan (50ug/ml) as an amino-acid supplement. Mycophenolic acid (MPA) was dissolved in DMSO and diluted 1000 fold into working concentrations in liquid and pad conditions. IPTG and xylose were dissolved in H_2O and diluted 1000 fold and 12.5 fold respectively into working concentrations. Concentrations of 0.1% DMSO were not found to affect cell growth or σ^B activity.

Mycophenolic Acid (MPA) experiments (Fig 1, S1-S6, S16)

Liquid snapshots: Cells were grown from glycerol stocks in SMM to mid-log (OD 0.3-0.8), then diluted back into SMM to an OD of 0.01. After regrowing to OD 0.1 at 37C , the culture volume was split and

varying concentrations of MPA (MP Biomedicals cat #194172), dissolved in 1000 fold DMSO concentrate, were added to separate cultures. After 2 hours of MPA exposure, cells were imaged as described above.

Time-lapse microscopy: Protocol was similar to liquid snapshot protocol above, except when cells regrew to OD 0.1, cells were then spotted on SMM 1.5% low melt agarose pads containing various concentrations of MPA. MPA pads were prepared by taking 1 mL of the SMM/agarose mixture and adding it to 1 μL of various MPA stock concentrations. After allowing cells to equilibrate after 2-3 hours, time-lapse acquisition was started.

Filament experiments (Fig 2, S7, S8)

Liquid snapshots: In the conditional filamentation strain, *ftsW* expression is controlled by the amount of IPTG in the culture. Long cells result from low expression of FtsW, and thus low levels of IPTG yield longer cells. In order to maintain wild-type cell length, cells were grown from glycerol stocks in SMM + 1mM IPTG to mid-log, then diluted back into SMM + 1mM IPTG to an OD of 0.01. After regrowth to OD 0.1, cells were washed with several exchanges of SMM without IPTG, and the resulting culture was re-diluted to OD 0.025 with varying levels of IPTG (0, 20, 30 1000 μM). After 3.5 hours of growth at 37C, MPA was added to a final concentration of 40 μg/mL and cells were grown for 3 hours. Cells were then imaged as described above.

Time-lapse microscopy: Initial growth steps were similar to above. Cells were grown from glycerol stocks in SMM + 1mM IPTG to mid-log, then diluted back into SMM + 1mM IPTG to an OD of 0.01. After regrowth to OD 0.1, cells were washed with several exchanges of SMM without IPTG, and the resulting culture was re-diluted to OD 0.025 with either 20 or 1000 μM IPTG. After 3h of growth at 37C, cells were washed and spotted on pads. For experiment in Fig. S8D pads contained 40 μg/mL MPA and either 0 μM IPTG (for long cells) or 1000 μM IPTG (for short cells). For experiment in Fig. 2A and S8E, pads contained 0 μM IPTG and varying levels (0, 10, 20, 40, 80) μg/mL of MPA. After allowing cells to equilibrate after 1-2 hours, time-lapse acquisition was started.

Closed-loop sensitivity measurements (Fig 2C and S11)

Cells were prepared similarly to previous experiments. Upon regrowth to OD 0.1 in SMM, culture volume was split and varying levels of IPTG (0, 10, 20, 30, 40, 50, 1000 μM) were added to separate cultures. After 90 minutes of growth, cells were spotted on PBS 1.5% agarose pads and imaged. Matlab software was used to generate the composite scatter plot (Fig. 2C), and fit it to a standard Hill function equation.

Open-loop experiment (Fig 3)

Upon regrowth to OD 0.1 in SMM, cells were spotted on SMM pads. Xylose was pipetted on the tops (non-cell side) of the 6mm pads to give a saturating concentration of xylose (2%). Time-lapse acquisition was started ~1 hour after exposure to xylose. After microcolonies reached the size of ~8 cells (~2h), the lid to the Willco dish was removed and varying levels of IPTG (0, 6, 15, 30, 60, 1000 μM) were pipetted on to separate pads. Time-lapse acquisition was then continued.

Closed-loop experiment (Fig. 4)

Upon regrowth to OD 0.1 in SMM, cells were spotted on SMM pads. Various levels of IPTG were added to the pads (0,2,3,4,5,7.5 μM IPTG). After allowing cells to equilibrate after ~1 hours, time-lapse acquisition was started.

Quantitative PCR (Fig S7)

Strain JJB712 was grown in triplicate to mid-log from glycerol stocks in SMM minimal media + 1 mM IPTG in order to maintain FtsW expression. Cells were then diluted back into SMM + 1mM IPTG to an OD of 0.01. After regrowth to OD 0.1, cells were washed with several exchanges of SMM without IPTG, and the resulting cultures was re-diluted to OD 0.025 with either 0 or 1000 μM IPTG. Cells were allowed to grow to an OD of 0.25 before harvesting. RNA from 1mL of culture was extracted using the Qiagen RNeasy Protect Bacteria Mini Kit(#74524), using 5 mg/ml lysozyme for cell lysis.

0.5 ug of RNA was reverse transcribed using the Biorad iScript One-Step RT-PCR Kit for Probes. Quantitative PCR was performed on a BioRad CFX96 Real Time System using 1/1000th of the cDNA reaction, single gene qPCR primer/probe mixtures from IDT (see table below), and BioRad SsoFast Probes Supermix, in a final volume of 20μl. Each gene for each biological replicate was analyzed in triplicate and averaged to obtain the C(t) value for each gene.

Gene expression was measured relative to mCherry, whose mean fluorescence per cell was measured to be consistent between long and short cells (see Figure S7A). An additional housekeeping gene (rrnD) was also included for comparison and yielded qualitatively similar results. To compute the ratio of long cell to short cell gene expression, each long cell biological replicate (9 total across three days) was compared to the mean short cell expression for each day. These 9 points were averaged and error was calculated for each gene and plotted (see Figure S7B).

Quantitative PCR primer/probe sequences

Gene	Forward Primer	Reverse Primer	Probe
mCherry	CAG GTT TCT TGG CTT TGT ACG	AAA AGA CGA TGG GTT GGG AG	**HEX** - AT GTA TCC GGA AGA TGG TGC GCT G
rrnD	GCC CTT TGT TCT GTC CAT TG	ACC CTT GAT CTT AGT TGC CAG	**HEX** - CG TCA TCC CCA CCT TCC TCC G
rsbQ	AAG AAC ATC CTG GGC ATA GC	GTT CGG GAC ATT CAG ATT TGC	**FAM** - CG CGC ATA TG ACC TGA ATC GTT ACC A
rsbP	TGC CGT GCT ATA TCA ATC TCG	TCT CAG CCC CGT TAA AGT TAT G	**FAM** - TG TGA AGG TG CCG GTC CAA TTC
rsbV	CCT TCA AGC CTG TAA TGT CAA AC	TGC CTG AAA GAT GTC AGC TAC	**FAM** - AA ACG CCC A A TCC GGT ACT GTC C
rsbW	CAT TAA ATA TAG ACC GAG CCC TCC	TTA GAG GTT ATT GTG GCG GAT G	**FAM** - TG ATC AAC TG TGT GCG AAG GTG TGT
sigB	TCT GAA AGG ACA TGA AGC ACG	AAG CCT TAT CCG TTG ACC AC	**FAM** - AG GAC GGA TA TGA GCG GGT CAA C
sigA	AGA TCA AGG AAC AGC ATA CCG	GAA ATC GCC TAC GCT CAA AAG	**FAM** - AG TAT CGC AA AAC GGT ATG TCG GAC G

Immunoblot analyses (Fig S10)

Strain JJB737 was grown at 37^{o}C in LB to OD_{600} of 0.2. The culture was divided into two equal volumes, and exposed to either 0 or 1mM IPTG. After 30 minutes of further growth, cells were pelleted by centrifugation at 3,000 x g for 10 minutes at 25^{o}C. Proteins were extracted by detergent lysis, using Thermo Scientific Y-PER Yeast Protein Extraction Reagent (Product No. 78991) according to the manufacturer's instructions. To prevent degradation of proteins, protease inhibitors (Thermo Scientific Halt Protease Inhibitor Cocktail, EDTA-Free, Product No. 87785) were added to the samples. Total protein concentrations were determined by a BCA Protein Assay (Thermo Scientific Pierce BCA Protein Assay Kit, Product No. 23227).

Immunoblotting of RsbQ: Samples (100 µg) of total proteins were resolved on NuPAGE® Novex® 4-12% Bis-Tris Gels (Invitrogen, Product No. NP0335BOX) with MES SDS running buffer at 150 V constant for 1 hour. After performing electrophoresis, proteins were transferred to nitrocellulose membranes (0.2 µm) by dry blotting using an iBlot® Gel Transfer Device (Invitrogen, Product No. IB1001). The blotted membranes were soaked in freshly prepared blocking reagent, which comprised of TBST (20 mM Tris base, 137 mM sodium chloride, 0.1% (v/v) Tween 20, pH 7.6), 5% nonfat dry milk, and 2% BSA, for 1 hour at room temperature with constant agitation. The blots were then incubated in a 1:10000 dilution of anti-RsbQ in fresh blocking solution for 2 h with agitation. The RsbQ polyclonal antibody was a gift of CW Price [7]. After washing in TBST 3 times for 10 min each time, the blots were incubated with a 1:2000 dilution of the secondary antibody (ECL Rabbit IgG, HRP-Linked Whole Ab from donkey, Product No. NA934-100UL) in fresh blocking solution for 1 hour. The blots were then washed in TBST 3 times for 5 min each time, followed by a 30 minutes final wash. SuperSignal West Pico Chemiluminescent Substrate (Thermo Scientific, Product No. 34077) was used for horseradish peroxidase detection according to the manufacturer's instructions.

Protein bands were visualized on a VersaDoc gel imaging system (Bio-Rad Laboratories).

Immunoblotting of RsbV and RsbVp: Proteins extracts were processed with Pierce Detergent Removal Spin Columns followed by Zeba Desalt Spin Colums (Thermo Scientific, Product No. 87778 and 89889) according to the manufacturer's instructions. 200 µg of total proteins were separated by two-dimensional electrophoresis according to the carrier ampholine method of isoelectric focusing [8-9] by Kendrick Labs, Inc. (Madison, WI) as follows: Isoelectric focusing was carried out in a glass tube of inner diameter 2.3 mm using 2% pH 3.5-10 mix4L Servalytes, (Serva, Heidelberg, Germany) for 9600 volt-hrs. One µg of an IEF internal standard, tropomyosin, was added to the sample. This protein migrates as a doublet with lower polypeptide spot of MW 33,000 and pI 5.2. The enclosed tube gel pH gradient plot for this set of Servalytes was determined with a surface pH electrode.

After equilibration for 10 min in Buffer 'O' (10% glycerol, 50 mM dithiothreitol, 2.3% SDS and 0.0625 M tris, pH 6.8), each tube gel was sealed to the top of a stacking gel that overlaid a 10% acrylamide slab gel (0.75 mm thick). SDS slab gel electrophoresis was carried out for about 4 hrs at 15 mA/gel. After slab gel electrophoresis, the gel was placed in transfer buffer (10mM Caps, pH 11.0, 10% methanol) and transblotted onto a PVDF membrane overnight at 200 mA and approximately 100 volts/ two gels.

The PVDF membranes were destained with 100% methanol, rinsed with TBST and blocked as described above. The membranes were incubated overnight at 4^{o}C in a 1:50 dilution of anti-RsbV in fresh blocking solution with constant agitation. The RsbV monoclonal antibody was a gift of WG Haldenwang (described in [10]). The secondary antibody was used at a 1:2000 dilution (ECL Mouse IgG, HRP-Linked Whole Ab from sheep, Product No. NXA931). SuperSignal West Pico Chemiluminescent Substrate was used for detection as described above.

Statistical sampling

To understand whether a relationship existed between pulsing in sister and parent-child cells, only cell-lineages that successfully divided into two continuous daughter cells were sampled and analyzed for pulses. In these lineages, it was not required that a pulse was present. 'Twin' pulses occurred if at least one pulse occurred in both daughter cells of each cell lineage, where a 'parent-child' pulse occurred if a pulse occurred in at least one of the daughter cells of a parent who also pulsed.

To compare these results to an expected value, the pulse frequency of daughter cell was used to create a randomized set of pulsing in each daughter cell for the same number of analyzed lineages as found in the final data set. Each trial involved randomization of daughter cell pulsing, and a subsequent twin pulse frequency calculation. This was done 50000 times, and the resulting distribution of twin pulses was plotted as a histogram in Fig. S3.

For parent-child pulses, expected value distributions were created by randomizing both whether a parent pulsed, and whether at least one child pulsed, using measured pulse frequencies in each of these populations. As in the sister-cell analysis, 50000 trials were performed.

Quantitative Analysis

Quantitative movie analysis used custom image analysis code in MATLAB, similar to that previously described [11]. Briefly, we segmented fluorescence images of the P_{trpE} -mCherry constitutive reporter using edge detection to identify individual cells. Segmented cells were tracked semi-automatically from frame to frame on the basis of position and orientation. Fluorescence was defined as the sum of pixel intensities within the area of the cell. Calculation of promoter activity, and analysis of pulse statistics, were carried out using custom Matlab code, described below

<u>Promoter Activity definition</u>

Promoter activity is defined as the rate of protein production. We extract this quantity from time-lapse data by considering the production, degradation, photobleaching, and dilution rates of the fluorescent protein. Flourescent protein production occurs at a rate *P(t).* We combine all the degradation, dilution, and photobleaching processes into a first-order effective degradation rate constant, denoted γ. Thus, production rate of a Fluorescent protein, *F*, is given by:

$$\frac{dF(t)}{dt} = P(t) - \gamma F(t)$$

To solve for $P(t)$ requires differentiating the total fluorescence $F(t)$, but this process is sensitive to cell segmentation errors. To circumvent this problem, we rewrite the cell's total fluorescence $F(t)$ in terms of is its mean fluorescence, $M(t)$ multiplied by its area, $A(t)$:

$$F(t) = A(t)M(t)$$

The area is equal to the width ($W(t)$) of the cell multiplied by its length ($L(t)$). As the width of *B. subtilis* cells are effectively constant, we can rewrite this equation as:

$$F(t) = L(t)M(t)$$

Where we suppress the constant width value W_0. Replacing $F(t)$ in promoter activity definition with this term, and using the differentiation chain rule we obtain:

$$\tilde{P} = \frac{P(t)}{L(t)} = (\mu(t) + \gamma)M(t) + \frac{dM(t)}{dt}$$

Where we define $\mu(t) = \frac{dlogL}{dt}$ as the cell's instantaneous growth rate. $\tilde{P} = \frac{P}{L}$ can be interpreted as the production rate per chromosomal equivalent, allowing comparison of production rate throughout all points in the cell cycle. To avoid unphysical negative values of promoter activity due to bleaching of fluorescent proteins during the movie, we set γ=0.05 for all movies analyzed in this work. Promoter activity depends only on the mean cell fluorescence and length which are continuous values that are relatively independent of the exact segmentation of the cell. Nevertheless, small changes in cell segmentation from frame to frame still occur, which can affect length and mean fluorescence measurements. Length and mean fluorescence signals were therefore smoothed using a standard first order locally weighted algorithm (the MATLAB smooth function with Lowess algorithm).

Colony promoter activity, as calculated in Fig. 3 and S14, is defined as the amount of protein produced per unit colony area. Unlike in single cells, here the relative impact of potential segmentation errors is strongly reduced by averaging over the entire colony. We defined colony promoter activity as

$$P_{colony} = \frac{1}{A(t)} \frac{dF_{tot}(t)}{dt}.$$

Here, $A(t)$ represents total colony area in pixels, and F_{tot} is integrated fluorescence over the entire colony.

Calculation of Pulse statistics

We characterized the amplitude, duration and frequency of the pulses using custom Matlab software. Peak locations were found by locating the local maxima of the traces of P_{sigB}-YFP promoter activity. We defined the start and end of the pulse by locating the local minima surrounding the peak. The pulse amplitude and duration were obtained by calculating the pulse height and half-maximum width, respectively. Pulse frequency was defined as the number of pulses per hour. To prevent erroneous

detection of non-pulse fluctuations in the traces, we imposed two criteria for pulse detection: First, we rejected pulses below a minimum amplitude cutoff. Second, we rejected pulses which contributed less than thirty percent of total gene expression over their duration, i.e. pulses that were relatively small compared to the basal expression rates.

The full σ^B network has energy and environmental stress inputs

In wild-type *B. subtilis*, RsbV can be dephosphorylated by two distinct pathways. Energy stresses activate through RsbP and its co-regulator RsbQ, while under environmental stresses use RsbU and its co-regulator RsbT [12]. For both systems, dephosphorylated RsbV then binds RsbW, releasing σ^B to activate downstream target genes, including regulating its own operon.

The environmental stress pathway contains additional regulatory components that do not control the response in energy stress. In particular, a ~1.8 Mda supramolecular complex, called the stressosome [13], regulates activation of σ^B in response to diverse stresses including ethanol, acid, heat, and osmotic stress, by controlling the activity of the RsbU phosphatase . Structurally, the stressosome is composed of several units of RsbR and RsbS, which control the availability of the kinase, RsbT, the co-activator of RsbU. Interestingly, the activation of RsbU is controlled through another partner switching mechanism [14]. In the resting (no stress) state, RsbS is found unphosphorylated and complexed to RsbR and RsbT in the stressosome. Stress increases the kinase activity of RsbT, driving the phosphorylation of RsbS, an event that correlates with the release of RsbT from the stressosome. How RsbT kinase activity increases is unknown, but RsbR may mediate an increase in activity [15]. Once released, RsbT is free to interact with RsbU and activate it.

In additional to upstream components that are unique to the environmental stress pathway, the activation of σ^B results in additional expression of an environmental specific regulator, the phosphatase RsbX. RsbX acts upon the stressosome to dephosphorylate RsbS and RsbR [16], counteracting the self-activation of RsbT and blocking further activation from the environmental stress pathway. In this study we focus on the energy stress pathway, and work in a background in which the environmental stress pathway sensor, rsbU, is removed to avoid cross-talk between pathways. Therefore, while *rsbX* is present in the wild-type operon, we have omitted it for simplicity in the circuit diagram (Fig. 1B).

Pulse generation does not appear to involve excitability

We note that the wild-type system does not appear to behave like a classical excitable system [17]. In such systems, threshold-crossing fluctuations generate stereotyped pulses. The amplitude of such pulses are relatively independent of the characteristics of the triggering fluctuation, leading to a unimodal distribution of pulse amplitudes. In contrast, the wild-type σ^B system exhibits a monotonically decreasing distribution of pulse amplitudes for each MPA condition (Fig. 1F). This characteristic is reproduced in the model (Fig S19).

Minimal model of σ^B network

The gene regulatory network controlling σ^B is depicted in Fig. 1. For mathematical modeling, we simplified this network, concentrating on the minimal set of regulatory components required to explain both the experiments in Fig. 3 and, more generally, FM pulse generation. The purpose of this model is to demonstrate the effects observed, and not to model in detail the dynamics of the network. Here we combine the functions of RsbV and σ^B into a generalized activator, denoted A. Like RsbV, A is active in its unphosphorylated form, and inactive when phosphorylated (A_P). A phosphatase, functionally analogous to RsbQP and RsbTU complexes is denoted P. An RsbW-like Kinase, K, phosphorylates A. A activates itself and its inhibitor, K via a transcriptional autoregulatory positive feedback loop.

We assume Michaelis-Menten kinetics for the phosphorylation and dephosphorylation reactions. We also assume linear degradation and transcription rates. These assumptions result in the following continuous ordinary differential equations for the network. Note that phosphatase production rates are taken to be constant for any particular condition but were varied to analyze frequency modulation.

$$\frac{dA}{dt} = trans - phos + dephos - k_d A \qquad \text{S(1)}$$

$$\frac{dA_P}{dt} = phos - \ dephos - k_d A_P \qquad \text{S(2)}$$

$$\frac{dK}{dt} = trans \ - k_d K \qquad \text{S(3)}$$

Where:

$trans = \ t_a A + t_i$ is the transcription rate for both A and K. S(4)

$dephos = \frac{b_{dp} P A_p}{k_{dp} + A_p}$ is the rate of dephosphorylation. S(5)

$phos = \frac{b_p K A}{k_p + A}$ is the rate of phosphorylation of A. S(6)

In order to generate the observed ultrasensitivity, both phosphorylation and dephosphorylation reactions are assumed to operate in the saturated regimes. Although this matches well to the experimental data (Fig. 3, 4, S19, S20), we note that we do not rule out other sources of cooperativity, such as through the partner switching mechanism, or cooperative effects of protein binding [18].

For analysis of the effects of noise in phosphatase expression, P was replaced by a fluctuating time-series of phosphatase levels, $P(t)$ (see below). In equations S(1) and S(3), the transcription rates of A and K have been assumed exactly equal without loss of generality. This is because the dephosphorylation and phosphorylation rates of A are not controlled solely by the concentrations of P and K, but rather by $b_{dp}P$ and $b_p K$, respectively. Thus, changes in the relative transcription rates of the two proteins can be effectively accomplished by corresponding variation of b_{dp} and/or b_p. The transcription rate $trans$ is assumed to consist of two terms, t_i, a basal component representing leakiness from the promoter, and $t_a A$, representing the autoregulatory feedback due to A.

Parameters were chosen as follows:

Parameter	Description	Value
t_i	Basal transcription rate	0.005 μM/min
t_a	Autoregulatory (induced) transcription rate due to A feedback	0.025 min^{-1}
k_{dp}	A_P concentration (Michaelis constant) for half maximal dephosphorylation	0.1 μM
k_p	A concentration (Michaelis constant) for half maximal phosphorylation	0.1 μM
k_d	Degradation rate	0.005 min^{-1}
b_p	rate constant for phosphorylation	0.125 min^{-1}
b_{dp}	rate constant for dephosphorylation	0.065 min^{-1}

Open Loop Model , no noise (Fig. 3)

In the open loop model we modified the *trans* term to remove the transcriptional feedback, i.e. we set $trans = t_i$. This parameter t_i was then modulated to allow different protocols of operon induction. For each simulated operon level the system equations were numerically integrated in Matlab for 300 minutes using the built in ode45 solver. As in the experimental system, we assumed a constant phosphatase level ($P = 0.9\mu M$). For these simulations, t_i was initially set to zero and then switched to varying constant levels at 120 minutes, corresponding to the experimental operon induction conditions used in Fig. 3B.

Closed Loop model , with noise (Fig. 4)

To simulate noisy phosphatase expression in the closed loop model, we replaced the constant phosphatase level, P, with a time-varying phosphatase concentration, $P(t)$. $P(t)$ was pre-computed through a gamma distributed Ornstein-Uhlenbeck process [19]. Thus, it exhibited both a gamma distribution of concentrations [20-22], and an exponential autocorrelation function, with a correlation time roughly the order of the cell-cycle duration [11]. We chose a gamma distributed Ornstein-Uhlenbeck process, rather than a standard Ornstein-Uhlenbeck process as used in previous work [23], as there is strong evidence gene expression is gamma distributed in many systems [20-22], and because it permits independent modulation of burst size and frequency. The equations were numerically simulated using ode2, a fixed-step, 2nd order Euler method solver (http://www.mathworks.com/support/tech-notes/1500/1510.html). Discrete step sizes of 0.1 minutes were taken, to assure that the sampling rate was much faster than the timescale of the noise or of the pulses.

We modulated the burst size of the gamma distributed phosphatase in order to examine how phosphatase levels affect pulsing (Fig. 4). For each phosphatase level, we performed two hundred and fifty numerical simulations, each lasting twenty thousand minutes (simulated time), and used these data

to compute pulse statistics. We calculated the pulse duration, amplitude and frequency by examining the local maxima and minima of the simulated traces, using the same method as we used to determine pulse statistics from the experimental data.

Supplemental Movies

Movie S1

A time-lapse movie of strain JJB240, shown in Fig. 1D. Here a reporter for σ^B activity, P_{sigB}-YFP (shown in green), can be seen pulsing in response to exposure to energy stress, mycophenolic acid (60 μg/mL). Phase contrast images are shown in the background, in gray. The time between frames in this movie is 15 minutes.

Movie S2

The closed-loop strain (JJB643), shown in Fig 4D, S17, and S20, has a constitutive IPTG inducible phosphatase as the sole input to the σ^B system. By simply controlling the phosphatase levels (7.5 μM IPTG), σ^B activity displays similar pulsing dynamics to the wild-type system. Phase contrast images are shown in the background, in gray. The time between frames in this movie is 15 minutes. The reporter for σ^B activity, P_{sigB}-YFP, is shown in green.

References

1. Eldar, A., et al., *Partial penetrance facilitates developmental evolution in bacteria.* Nature, 2009. **460**(7254): p. 510-4.
2. Steinmetz, M. and R. Richter, *Plasmids designed to alter the antibiotic resistance expressed by insertion mutations in Bacillus subtilis, through in vivo recombination.* Gene, 1994. **142**(1): p. 79-83.
3. Vijay, K., et al., *A PP2C phosphatase containing a PAS domain is required to convey signals of energy stress to the sigmaB transcription factor of Bacillus subtilis.* Mol Microbiol, 2000. **35**(1): p. 180-8.
4. Boylan, S.A., et al., *Activation of Bacillus subtilis transcription factor sigma B by a regulatory pathway responsive to stationary-phase signals.* J Bacteriol, 1992. **174**(11): p. 3695-706.
5. Suel, G.M., et al., *Tunability and noise dependence in differentiation dynamics.* Science, 2007. **315**(5819): p. 1716-9.
6. Spizizen, J., *Transformation of Biochemically Deficient Strains of Bacillus Subtilis by Deoxyribonucleate.* Proc Natl Acad Sci U S A, 1958. **44**(10): p. 1072-8.
7. Brody, M.S., K. Vijay, and C.W. Price, *Catalytic function of an alpha/beta hydrolase is required for energy stress activation of the sigma(B) transcription factor in Bacillus subtilis.* J Bacteriol, 2001. **183**(21): p. 6422-8.
8. O'Farrell, P.H., *High resolution two-dimensional electrophoresis of proteins.* J Biol Chem, 1975. **250**(10): p. 4007-21.
9. Burgess-Cassler, A., et al., *Computerized quantitative analysis of coomassie-blue-stained serum proteins separated by two-dimensional electrophoresis.* Clin Chem, 1989. **35**(12): p. 2297-304.
10. Dufour, A. and W.G. Haldenwang, *Interactions between a Bacillus subtilis anti-sigma factor (RsbW) and its antagonist (RsbV).* J Bacteriol, 1994. **176**(7): p. 1813-20.
11. Rosenfeld, N., et al., *Gene regulation at the single-cell level.* Science, 2005. **307**(5717): p. 1962-5.

12. Hecker, M., J. Pane-Farre, and U. Volker, *SigB-dependent general stress response in Bacillus subtilis and related gram-positive bacteria.* Annu Rev Microbiol, 2007. **61**: p. 215-36.
13. Marles-Wright, J., et al., *Molecular architecture of the "stressosome," a signal integration and transduction hub.* Science, 2008. **322**(5898): p. 92-6.
14. Yang, X., et al., *Opposing pairs of serine protein kinases and phosphatases transmit signals of environmental stress to activate a bacterial transcription factor.* Genes Dev, 1996. **10**(18): p. 2265-75.
15. Gaidenko, T.A., et al., *Threonine phosphorylation of modulator protein RsbR governs its ability to regulate a serine kinase in the environmental stress signaling pathway of Bacillus subtilis.* J Mol Biol, 1999. **288**(1): p. 29-39.
16. Chen, C.C., M.D. Yudkin, and O. Delumeau, *Phosphorylation and RsbX-dependent dephosphorylation of RsbR in the RsbR-RsbS complex of Bacillus subtilis.* J Bacteriol, 2004. **186**(20): p. 6830-6.
17. Lindner, B., et al., *Effects of noise in excitable systems.* PHYSICS REPORTS- REVIEW SECTION OF PHYSICS LETTERS, 2004. **392**(6): p. 321-424.
18. Delumeau, O., R.J. Lewis, and M.D. Yudkin, *Protein-protein interactions that regulate the energy stress activation of sigma(B) in Bacillus subtilis.* J Bacteriol, 2002. **184**(20): p. 5583-9.
19. Barndorff-Nielsen, O.E. and N. Shephard, *Non-Gaussian OU based models and some of their uses in financial econometrics.* Journal of the Royal Statistical Society, B(Statistical Methodology), 2001. **63**: p. 167-241.
20. Taniguchi, Y., et al., *Quantifying E. coli proteome and transcriptome with single-molecule sensitivity in single cells.* Science, 2010. **329**(5991): p. 533-8.
21. Friedman, N., L. Cai, and X.S. Xie, *Linking stochastic dynamics to population distribution: an analytical framework of gene expression.* Phys Rev Lett, 2006. **97**(16): p. 168302.
22. Raj, A., et al., *Stochastic mRNA synthesis in mammalian cells.* PLoS Biol, 2006. **4**(10): p. e309.
23. Suel, G.M., et al., *An excitable gene regulatory circuit induces transient cellular differentiation.* Nature, 2006. **440**(7083): p. 545-50.

Fig S1

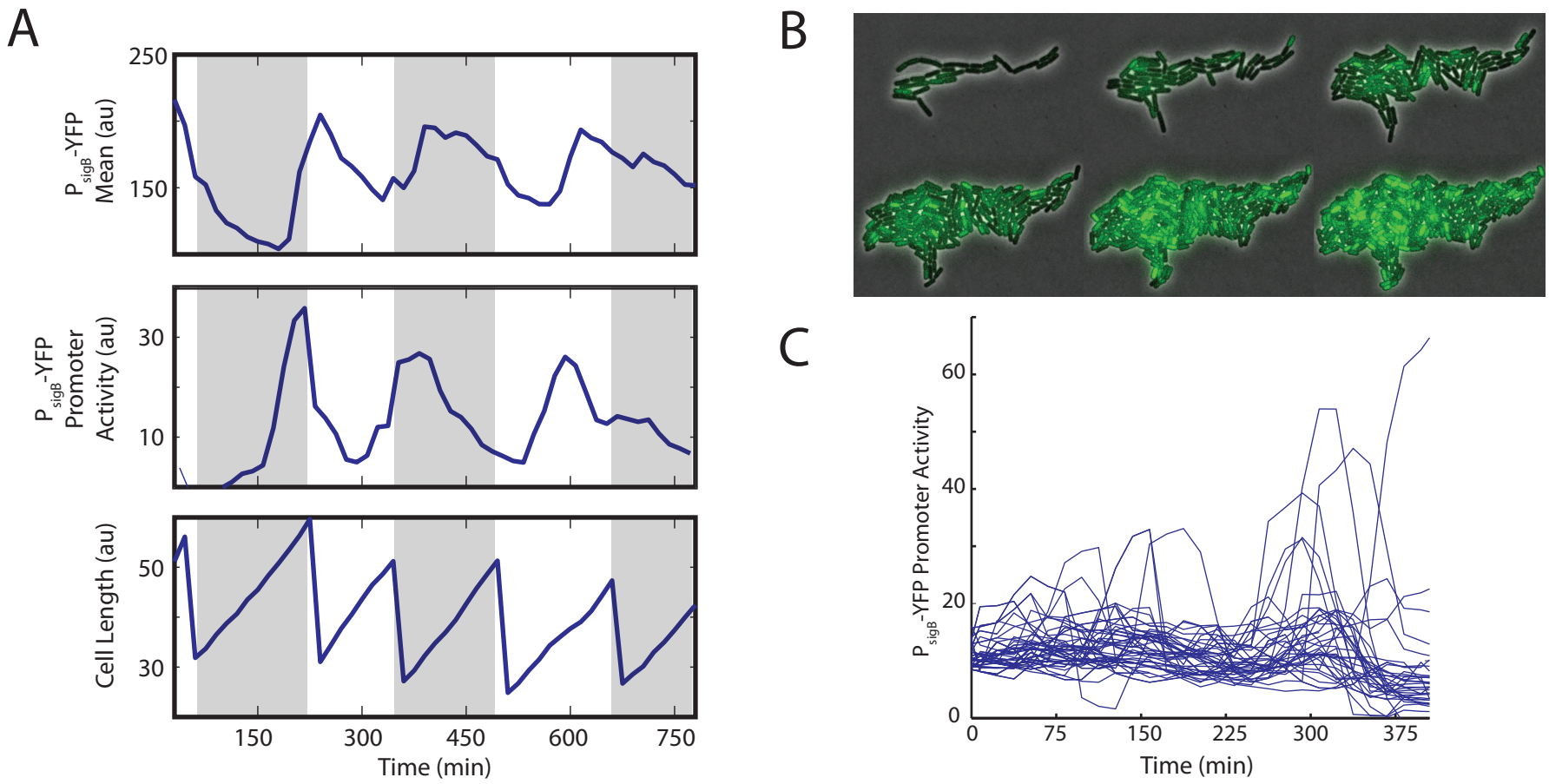

σ^B activity pulses under energy stress. (A) Example of cell lineage trace from a P_{sigB}-YFP reporter strain (JJB240, see strain list) exposed to 60 μg/ml MPA showing promoter activity (middle) calculated from the mean fluorescence (top) and the cell length (bottom). Alternating light/dark regions represent different cell cycles. (B-C) Cells also pulse under energy stress due to nutrient limitation / stationary phase. (B) Film strip of a time-lapse movie strain JJB240 grown on a LB/20 conditioned media pad mimicking stationary phase. Cells were grown to OD 1.8 and the resulting conditioned media was filtered from cells and made into low-melt agarose pads. Cells were then imaged on these conditioned pads (as described in supplementary methods). Colony images start from 450 min after the start of time-lapse to illustrate σ^B pulsing activity. (C) Cell lineage traces showing P_{sigB}-YFP promoter activity from movie described in (B), where t=0 min corresponds to the beginning of the filmstrip. For clarity, every 8th cell trace is shown.

Fig S2

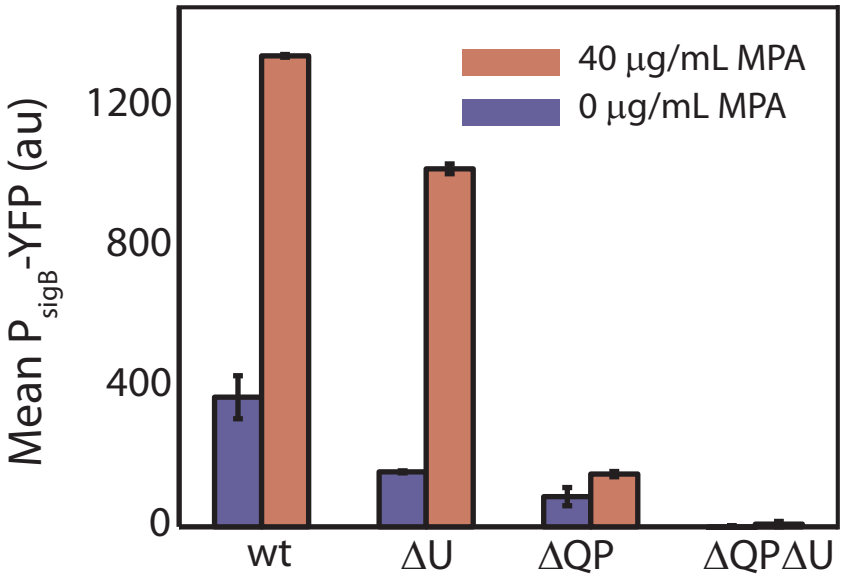

MPA induces σ^B activation through the RsbQP phosphatase. Wild-type (JJB213) and ΔrsbU (JJB240) strains, where the environmental stress phosphatase is deleted, strongly activate σ^B upon MPA exposure, in constrast to ΔrsbQP and ΔrsbQPΔrsbU strains without the RsbQP phosphatase (JJB629 and JJB461 respectively). Cells were grown in SMM and exposed to +/- 40 μg MPA for 150 minutes as described in supplemental methods. RsbU is the phosphatase that mediates environmental stress (see supplemental for full description of the σ^B network).

Fig S3

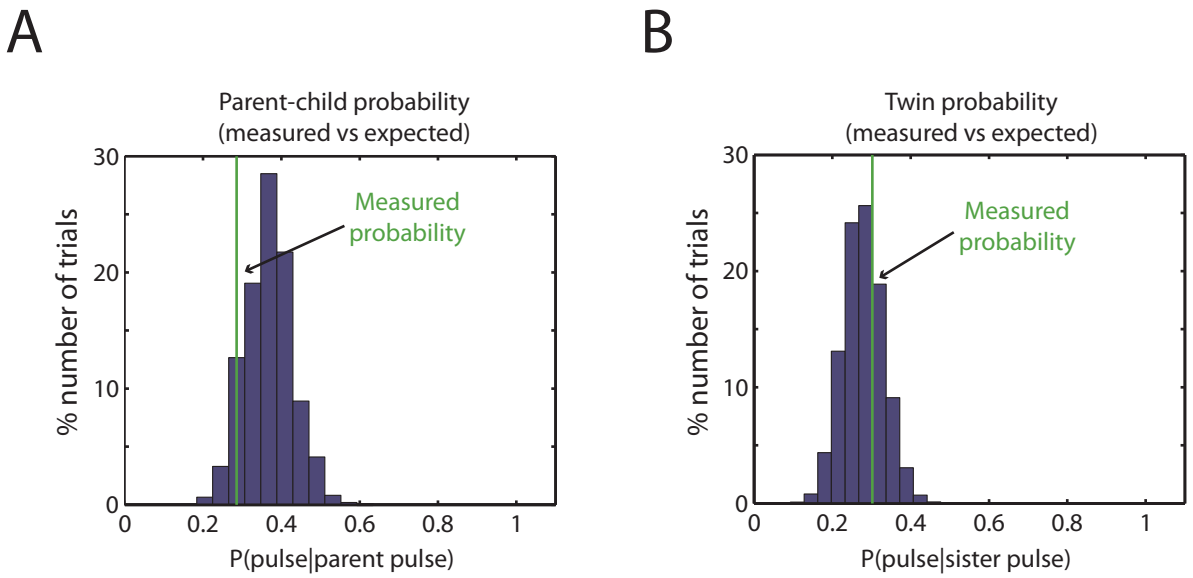

Pulse characteristics indicate σ^B pulses are stochastic. (A) The probability of pulses in generation *n+1* is independent of the presence of pulses in generation *n*. The frequency of instances where a parent and subsequent child pulsed (green line) was compared to a bootstrapped model (histogram) where parent/child pulses were randomized. (B) Pulse probability is nearly independent of the presence of pulses in sister cells. Green line indicates measured probability and can be compared to expected probabilities in a bootstrap model where sister cell pulses are randomized. For further descriptions of statistical methods, see Supplemental Methods.

Fig S4

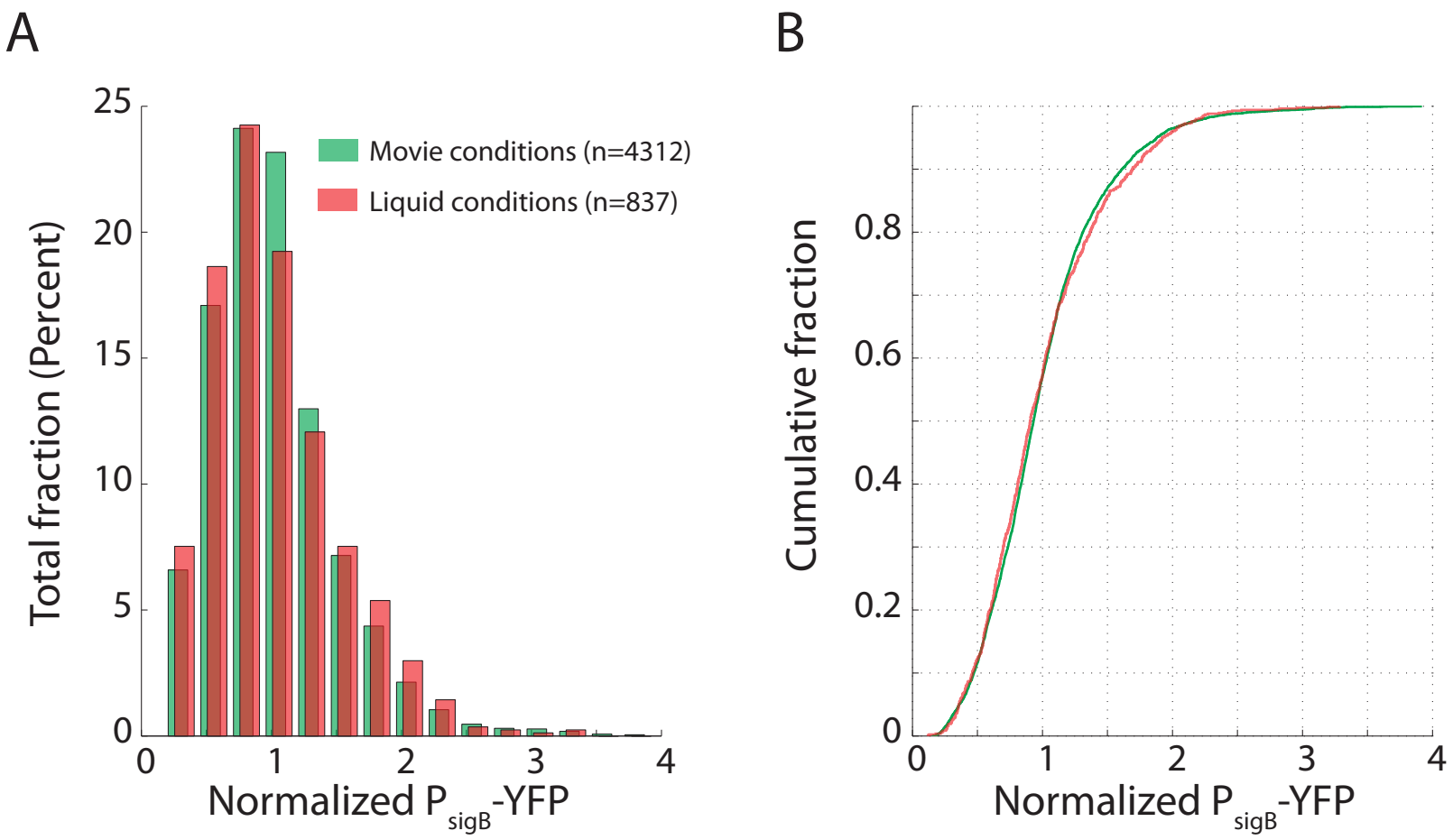

σ^B activity distributions exhibit similar variability in movies and liquid culture . (A) Mean single-cell P_{sigB}-YFP levels (shown in green) from strain JJB240 were extracted from individual frames of four time-lapse movies under 40 μg/mL MPA (from Fig. 1). Mean single-cell data were also acquired in liquid conditions after exposing cells to 40 μg/mL MPA in SMM (shown in orange). Data were corrected for autofluorescence using images of a strain containing no reporter construct (JJB176 (see strain list)) and mean normalized. (B) Cumulative distribution plots of movie and snapshot data shown in (A). A KS test showed that the differences between the distributions are not significant (p = 0.46).

Fig S5

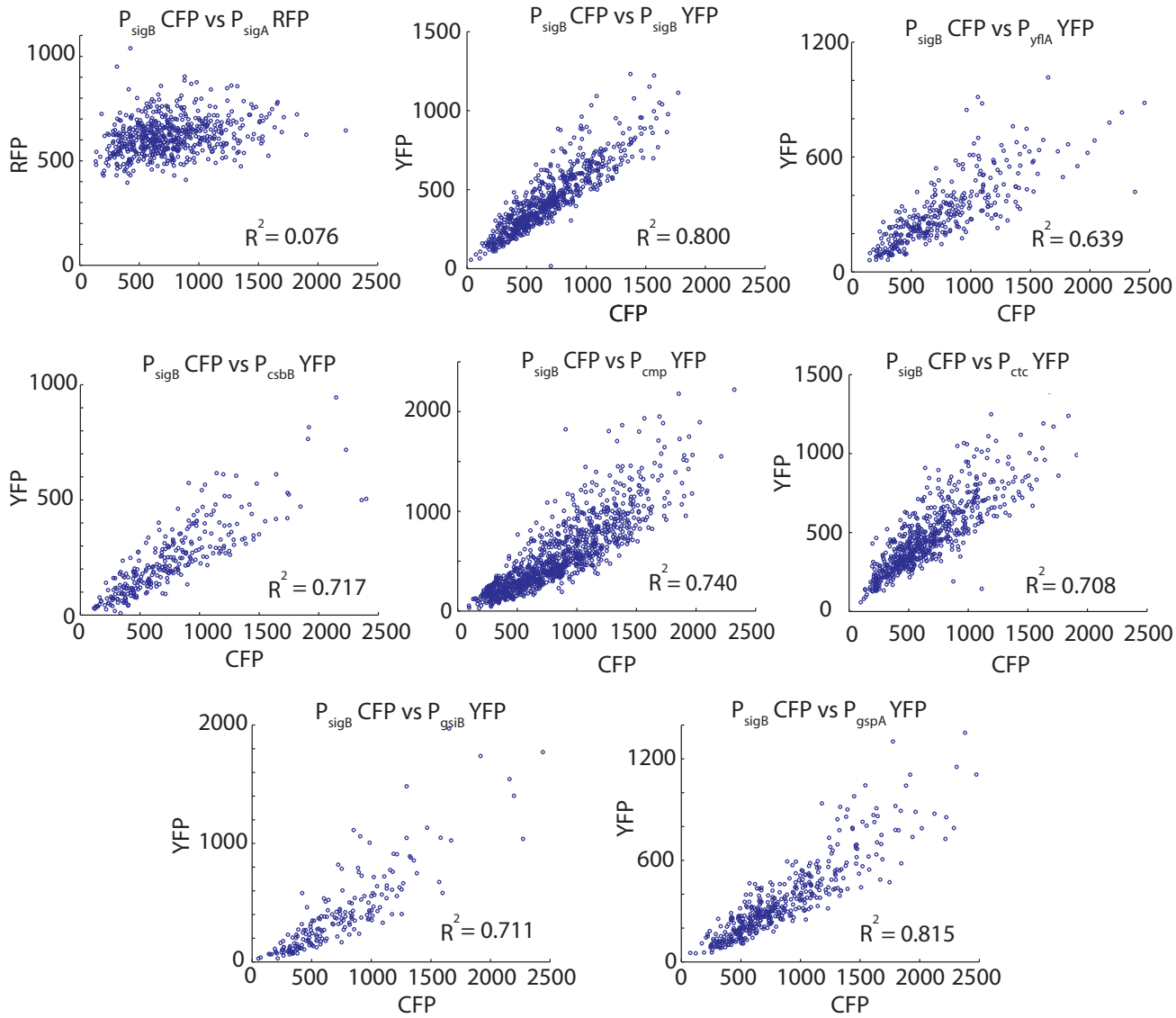

σ^B target genes are highly correlated at the single cell level. An independent YFP transcriptional reporter of σ^B activity was integrated into the *sacA* locus of an *amyE*::P_{sigB}-3X*cfp ppsB*::P_{sigA}-*mCh* reporter strain (JJB556-JJB572). Snapshots of gene expression were taken after growth in SMM liquid culture under 40 μg/mL MPA energy stress for 90 min. (Top left) P_{sigA}-mCh vs P_{sigB}-3XCFP. In this control, no correlation is observed between σ^B and a constitutive σ^A promoter. (B) (Top middle) P_{sigB}-YFP vs P_{sigB}-CFP. In this 'intrinsic noise' strain, YFP and CFP are values are highly correlated (high correlation coefficient (R^2)) showing that the variation in expression at the P_{sigB} promoter is due to global changes in σ^B activity. (Other plots) Different σ^B targets are also highly correlated with the P_{sigB} promoter.

Fig S6

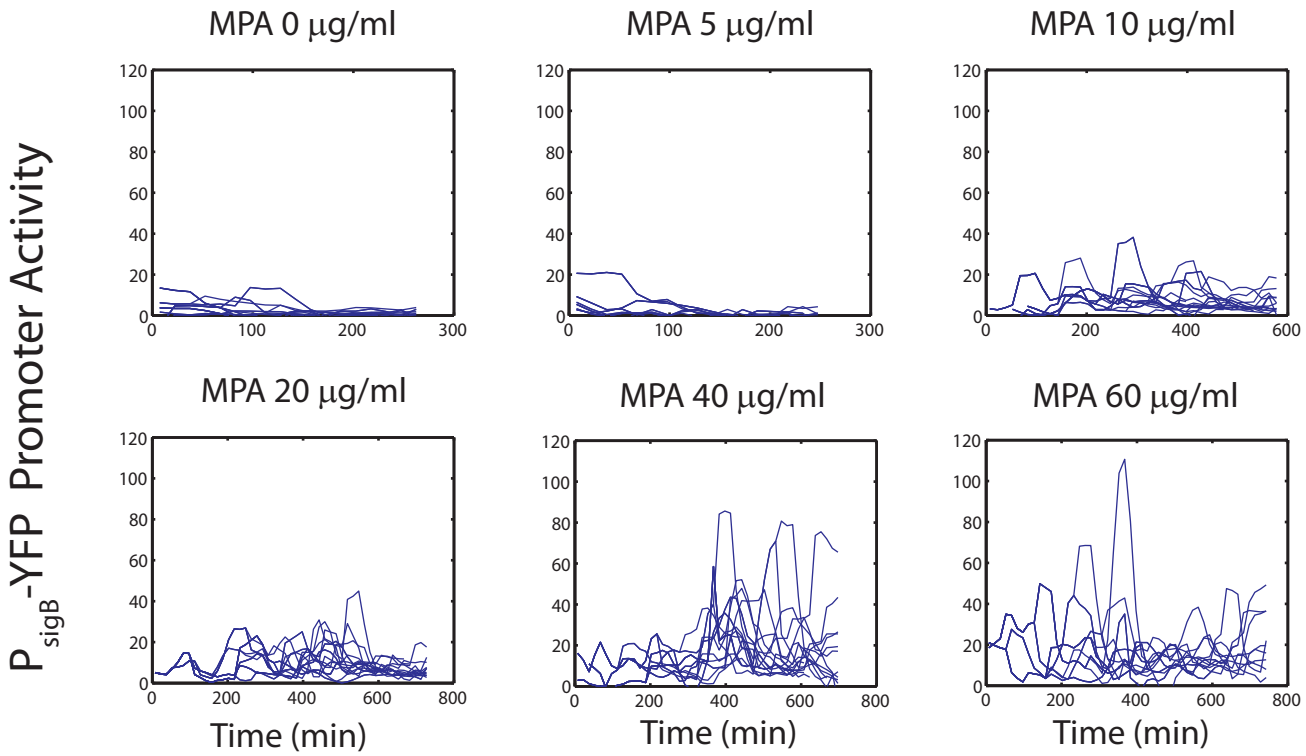

P_{sigB}-YFP promoter activity traces of individual cell lineages from movies acquired at various MPA concentrations. Cell lineage promoter activity traces of single movies from each MPA exposure. Pulse analysis of multiple movies comprise the data found in Figure 1C-F in the main text. Every 8th cell trace is shown for clarity. For full time-lapse microscopy methods, see supplementary.

Fig S7

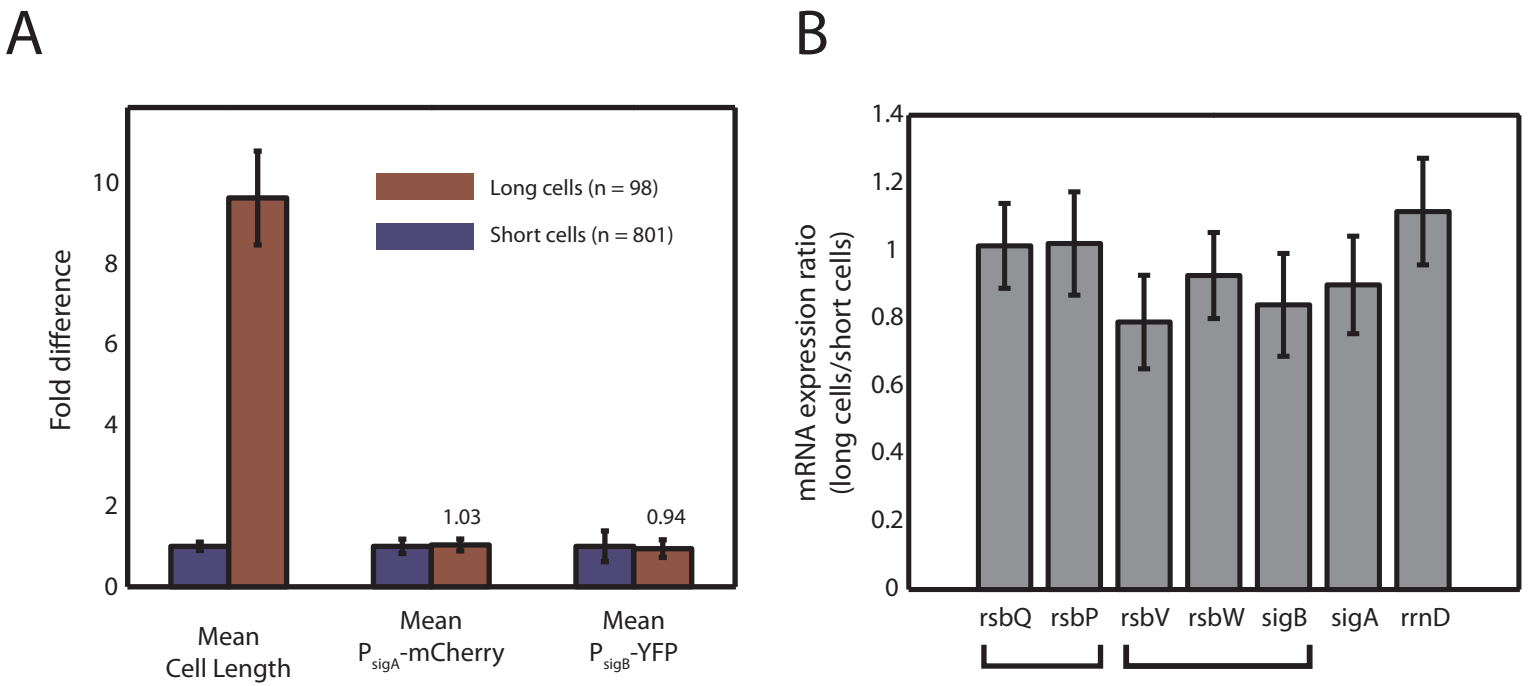

RNA expression is consistent with fluorescent cell measurements in filamented cells. (A) Using strain JJB712, long filamented cells (red bars) show similar mean expression of P_{sigA}-mCh and P_{sigB}-YFP compared to wild-type cells (blue bars, each normalized to 1), despite 10-fold longer mean cell length. Standard deviations are shown on bar plots (red bars are ratios to the wild-type values). (B) Histograms showing mRNA expression ratio of selected genes in long cells versus short cells, relative to mCherry expression, whose expression per cell volume was found to be constant (see A). Housekeeping and σ^B network components are expressed similarly in short cells versus long cells. Each measurement reflects data from three separate days, with three independent biological replicates. Standard deviations are shown on bar plots. Brackets show genes expressed from the same operon.

Fig S8

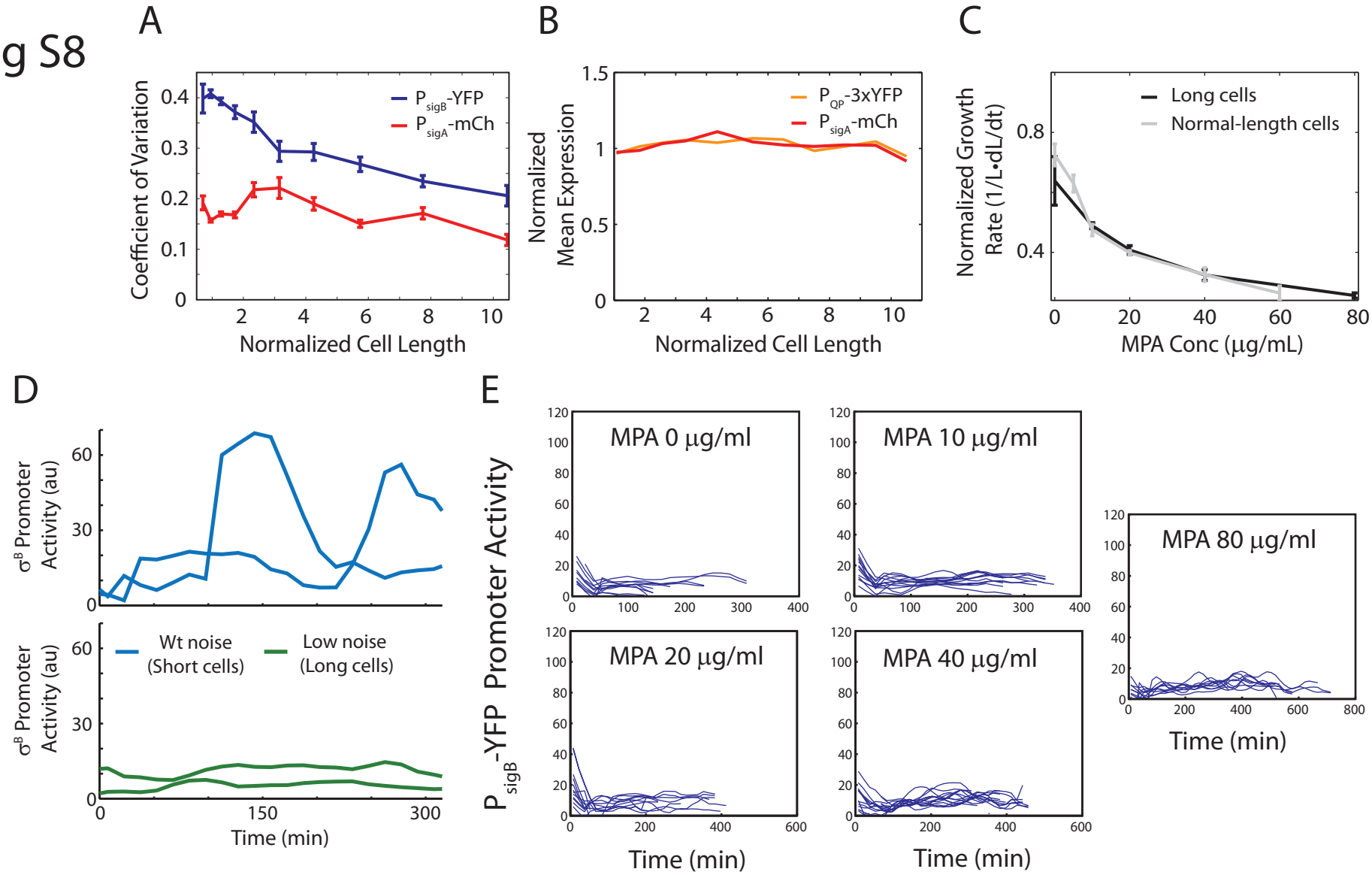

Reduced noise lowers P_{sigB}-YFP variability and reduces pulsing without changing QP phosphatase levels. (A) Plot of coefficient of variation of P_{sigB}-YFP activity (blue trace) or constitutive P_{sigA}-mCh reporter (red trace) versus normalized cell length in conditional *ftsW* filament strain (JJB712). At longer cell lengths P_{sigB}-YFP variability becomes comparable to that of the constitutive σ^A reporter due to a reduction in pulse frequency. (B) A reporter of phosphatase expression (orange trace) shows that mean phosphatase levels do not decrease with increasing cell lengths, similar to that of a constitutive control (red trace). Mean expression was normalized to the overall mean expression across all cell lengths for each reporter. (C) The physiological effect of MPA on growth rate is similar between long cells (black) and normal length cells (grey, strain JJB240)). (D)) σ^B activity traces from two cell lineages, in which septation was normal (short cells, top) or inhibited (long cells, bottom) at 40 µg/mL MPA. (E) Filament cell lineage promoter activity traces of single movies from each MPA exposure. Pulses in this strain are reduced compared to normal length cells (Fig. S6). Scale for the y-axis is set for comparison with data in Fig. S6.

Fig S9

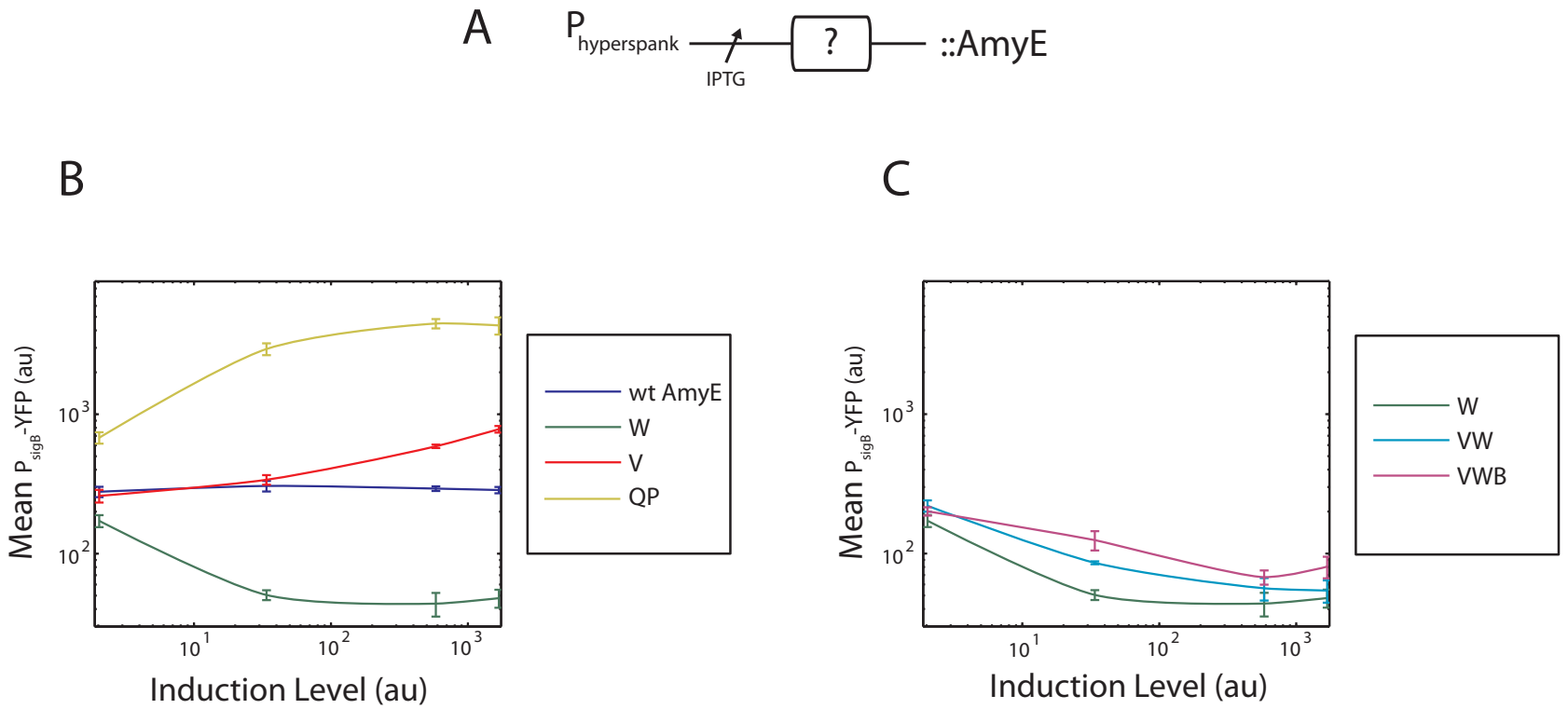

Ectopic expression of σ^B circuit components reveals sensitivity to phosphatase and kinase levels. (A) Diagram of genetic construct (for more details, see strain list). Each gene or gene combination (indicated by "X") was placed under the control of $P_{hyperspank}$ a strong IPTG-inducible promoter and integrated into the *amyE* locus. (B) Overexpression of RsbW, RsbV, RsbQP reveal that σ^B activity is most sensitive to kinase and phosphatase levels. Static snapshots of σ^B activity were taken 90 min after induction with various concentrations of IPTG. (C) RsbW exhibits a dominant negative effect over other operon components. Expression of fractional operon constructs containing RsbW alone, RsbVW, or RsbVWB were chromosomally integrated into the σ^B-YFP reporter strain. Despite the positive effects of RsbV and σ^B itself, inducing full operon RsbVWB repressed the system to almost the same level as expressing RsbW alone. In (B) and (C), induction level was measured by taking the mean expression of $P_{hyperspank}$-yfp (JJB432) at the same IPTG inducing concentrations.

Fig S10

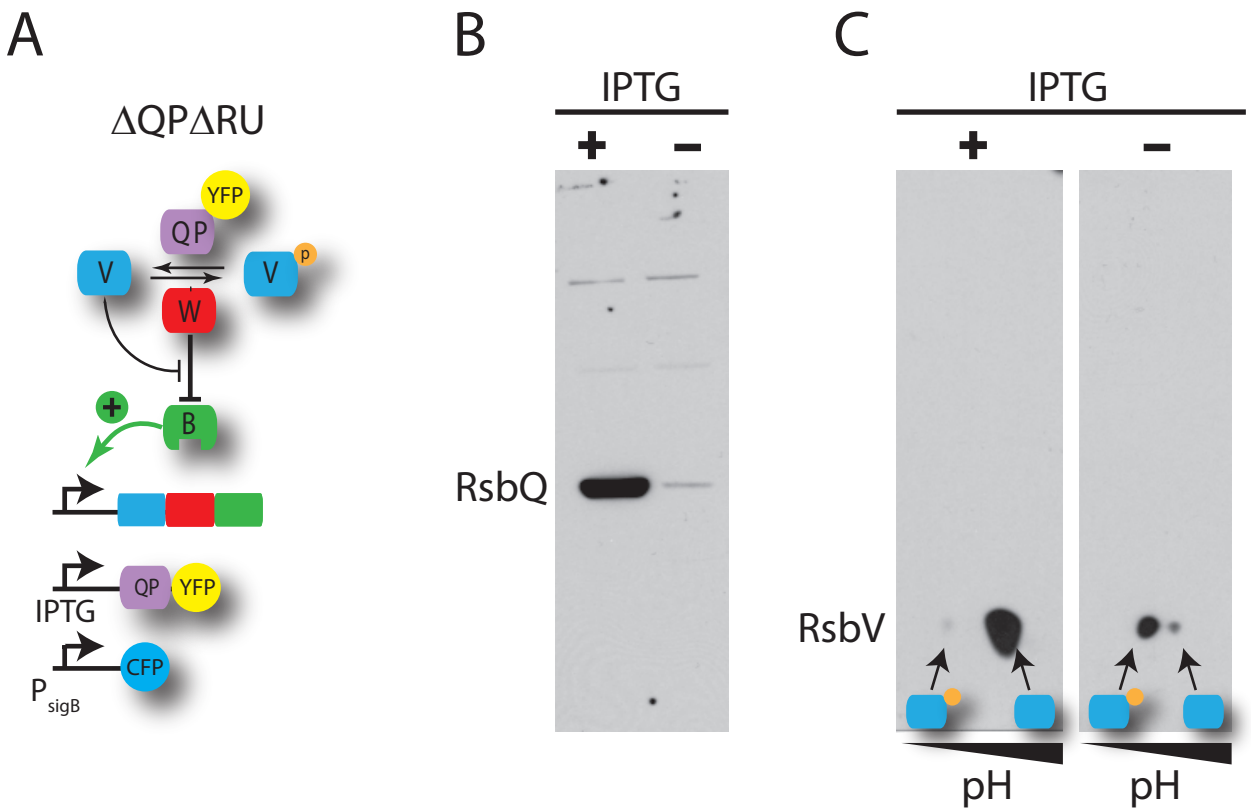

Upregulation of phosphatase QP-yfp increases phosphatase activity on RsbV substrate. (A) Strain JJB737 was grown in LB and phosphatase QP-yfp was induced with 1mM IPTG for 45 minutes. Cell lysates were extracted and used for western blotting. (B) Strong induction of the phosphatase RsbQ protein occurs with IPTG. 100 μg of cell lysate was loaded from each IPTG condition and blotted for the presence of RsbQ. The small amount of RsbQ present in the 'no IPTG' condition likely results from leakiness from the inducible promoter. (C) 2D Isoelectric/SDS electrophoresis was performed on cell lysates to separate the phosphorylated versus unphosphoryated forms of RsbV. Induction of ectopic phosphatase by IPTG switched RsbV from a predominantly phosphorylated state (right) to a state where RsbV was almost exclusively unphosphorylated (left).

Fig S11

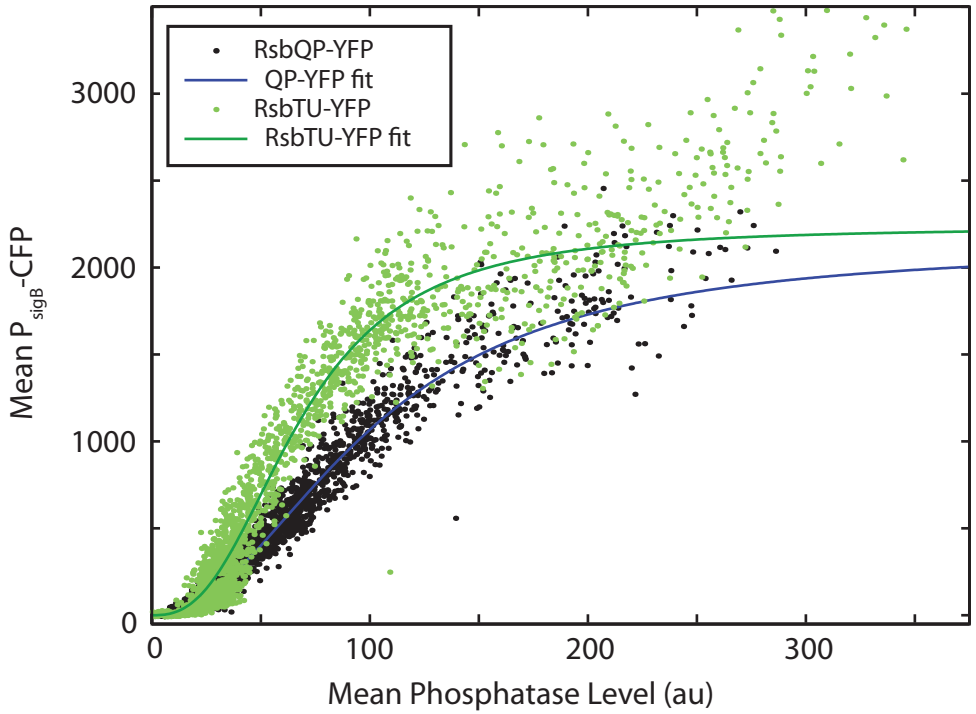

σ^B Activity is ultrasensitive to phosphatase expression. The yfp gene was fused to the C-terminus end of the rsbQP or rsbTU operon in the absence of other RsbV phosphatases. Dots represent individual cells where QP-yfp (black) or TU-yfp (green) was expressed to different levels and σ^B activity was measured using a P_{sigb}-CFP reporter via microscope snapshots. Hill fit (green and blue solid lines) estimate the hill coefficient as 2.12 (95% CI, n_{hill}=2.09-2.15) for QP-yfp and 2.62 (95% CI, n_{hill}=2.54-2.69) for TU-yfp. Data for QP-yfp here is shown in Figure 2C and is repeated for comparison to TU-yfp.

Fig S12

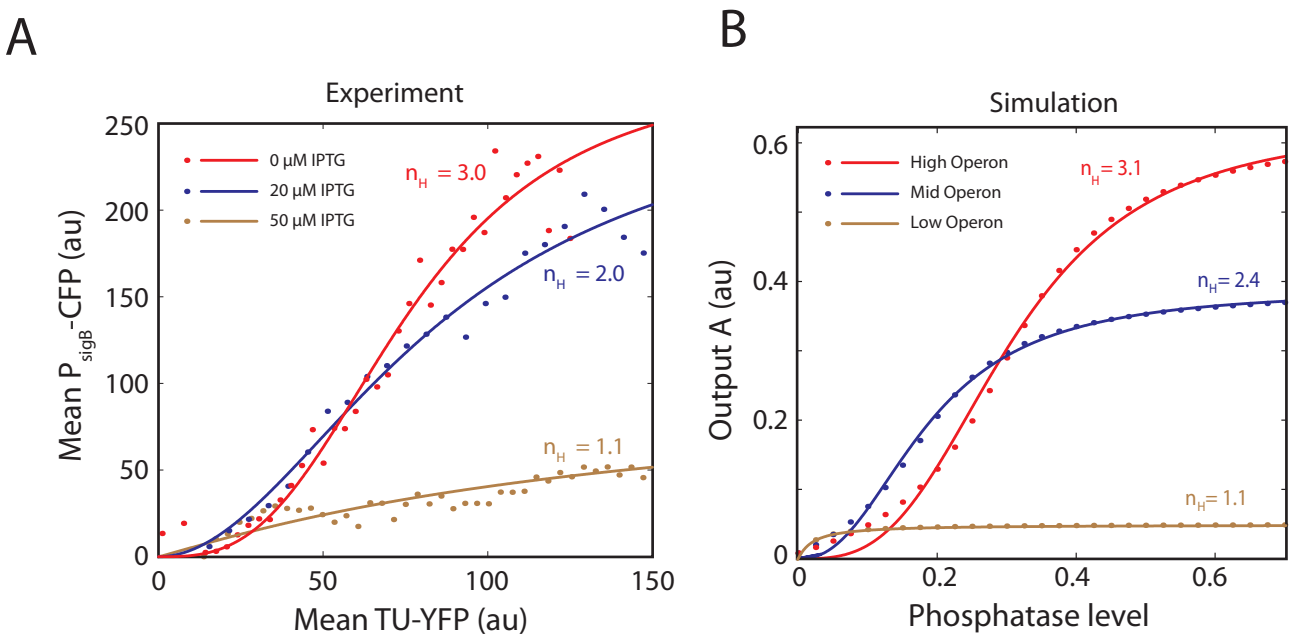

Ultrasensitivity is preserved in an open-loop system and increases with increasing operon expression. A strain expressing a xylose inducible phosphatase fused to yfp was integrated in a background where the σ^B operon was controlled by an IPTG inducible promoter (JJB749). Cells were spotted on SMM agarose pads with various IPTG concentrations (0, 20, 50 μM) to induce the operon to different basal levels. After 2.5 hours of equilibration, xylose (0.5, 1, 2, 4%) was added the different levels of IPTG to create a grid of conditions. After 1.5 hours of phosphatase induction, snapshots were taken. (A) Experimental data. Data were grouped according to IPTG concentration and sensitivity to phosphatase concentration was measured. Cells with similar phosphatase expression, as measured by yfp, were binned together and a hill function was fit to each IPTG concentration. The Hill coefficient is shown for each IPTG (operon level). (B) The open-loop simulation, (network diagram depicted in Figure 3C), shows that, like the experimental data, phophatase sensitivity increases with increasing basal operon expression.

Fig S13

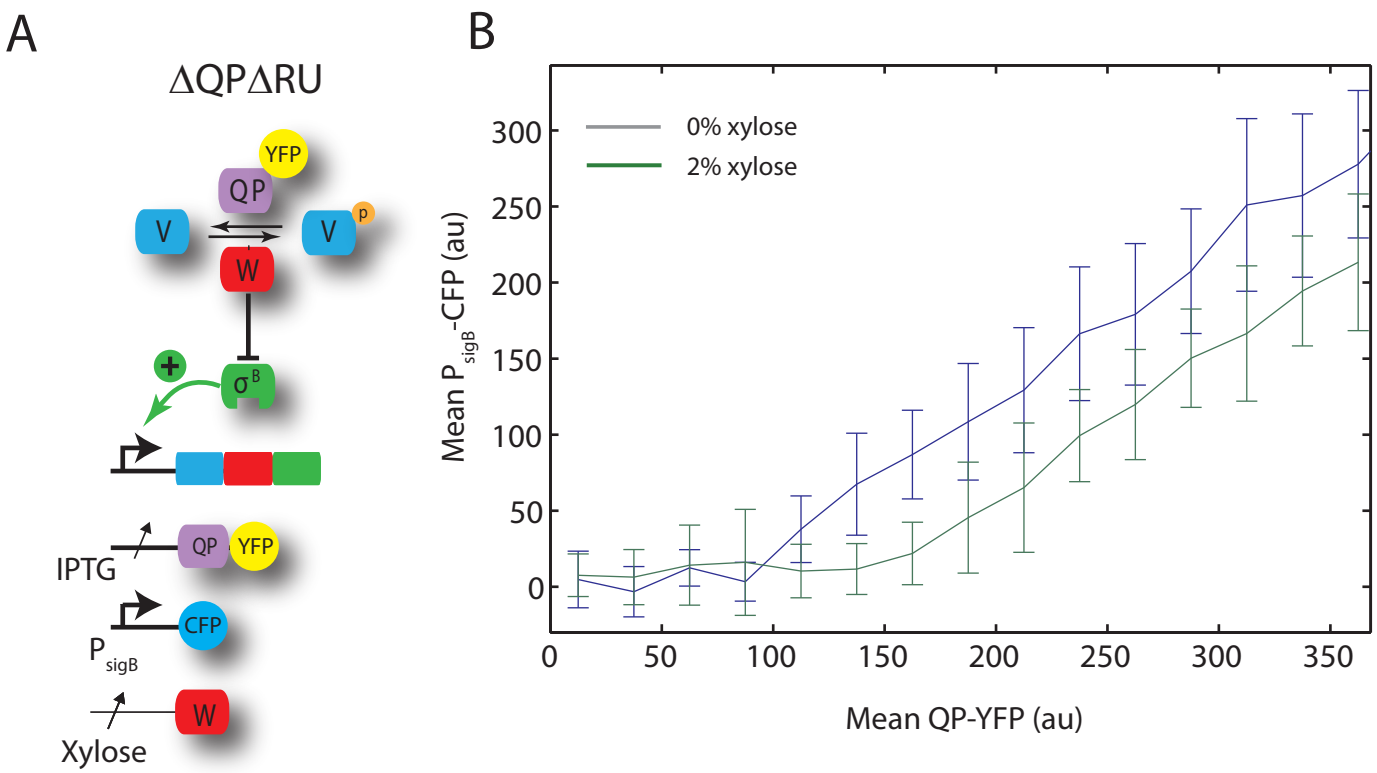

Balance between kinase and phosphatase sets threshold for σ^B activation. A) Strain JJB819 allows inducible control of both the kinase RsbW and phosphatase QP-YFP. In this experiment, first additional RsbW was induced by adding 2% Xylose. 2h later QP-YFP was then induced to varying levels by adding IPTG. 2h later snapshots of the resulting σ^B expression were taken. B) Upregulation of RsbW shifts the threshold for σ^B activation to higher levels of phosphatase. Cells with upregulated RsbW (2% Xylose, green line), require more QP-YFP expression to activate σ^B compared to uninduced cells (0% Xylose, blue line). Error bars represent standard deviation of single cell σ^B activity for a given QP-YFP level.

Fig S14

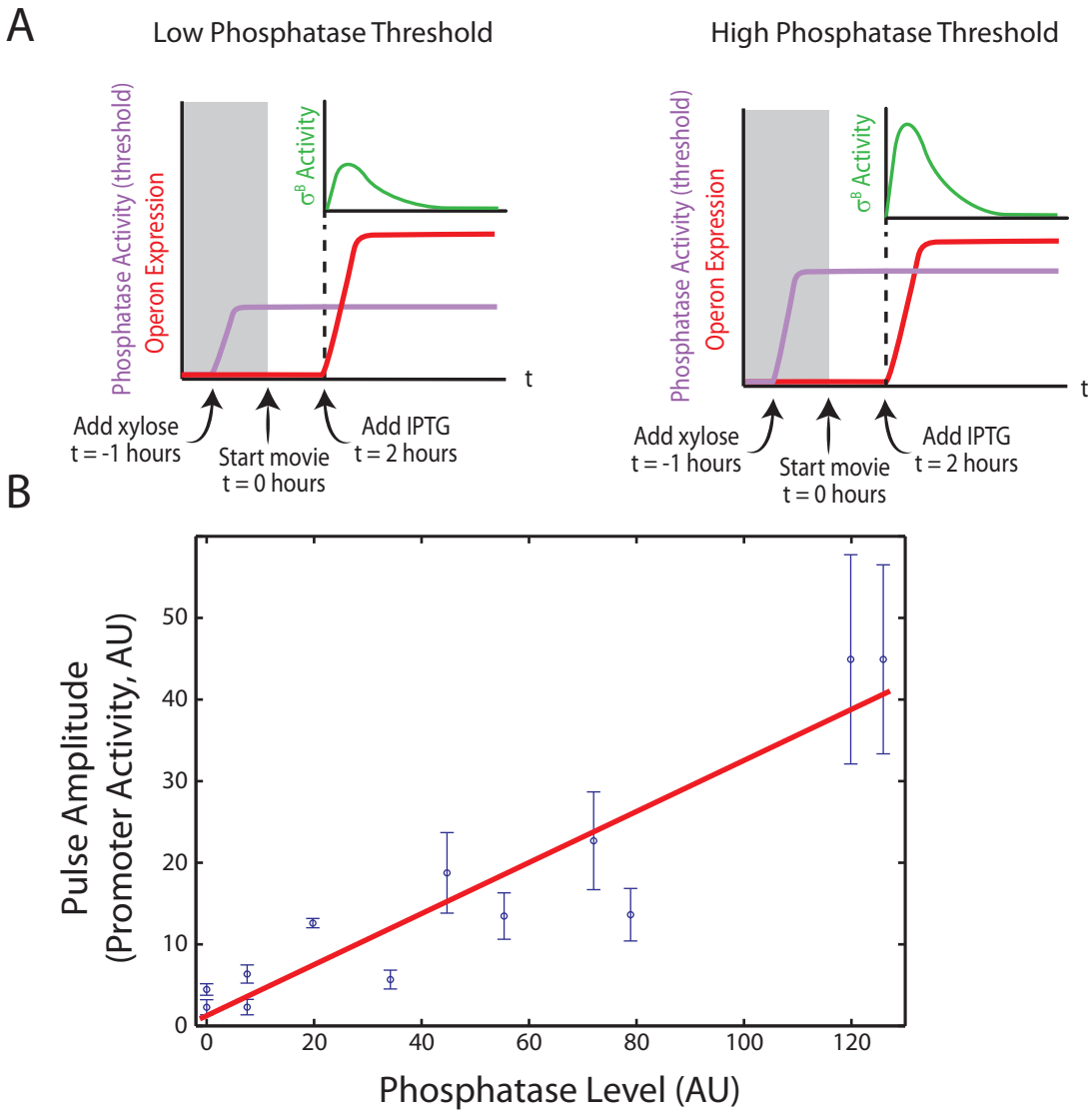

Pulse amplitude is proportional to phosphatase threshold. (A) Schematic of experimental protocol (modified from Figure 3, see open loop experiment description in Supplemental Methods). In order to test whether σ^B pulse amplitude increases with higher phosphatase threshold level, we preinduced the phosphatase RsbTU in strain JJB578 by adding xylose to varying levels (0%, 0.2%, 0.4%, 0.6%, 1.0%, 2.0% Xylose). After phosphatase had reached steady state levels, we then fully induced the σ^B operon (1 mM IPTG) and measured the resulting P_{sigB}-YFP activity via timelapse. (B) Pulse amplitude is proportional to the phosphatase threshold. Phosphatase level is estimated from the fluorescence values of a P_{sweet}-YFP reporter induced to the same level of xylose as the open loop strain. σ^B promoter activity is calculated from the mean fluorescence across the colony (see calculation of colony promoter activity in supplemental methods). Pulse amplitude for each data point represents an average amplitude from at least 3 movies on the same day, with error bars represent SEM. Two days of data are shown. Red line is unweighted linear fit (R^2 = 0.86).

Fig S15

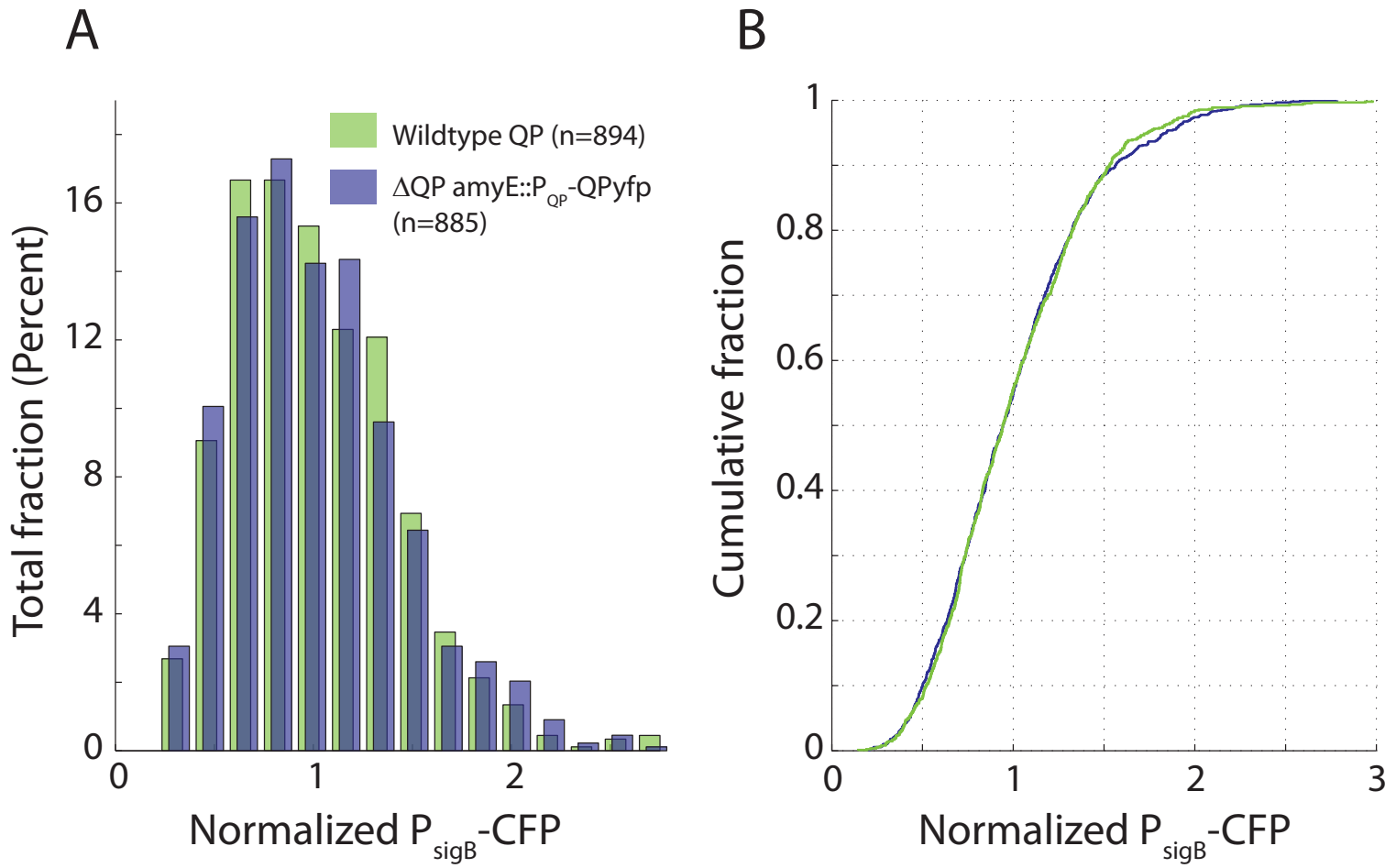

Expression of QP-yfp complements a QP deletion. (A) Expression of the phosphatase fusion protein QP-yfp from its endogenous promoter in the amyE locus (JJB739) produces similar mean-normalized σ^B activity distributions compared to wild-type QP (JJB781) upon treatment with 40 μg/mL MPA (blue and green respectively). Mean sigB activity under 40 μg/ml MPA in JJB739 was similar to wild-type QP (JJB781) (203 au (95% CI 201-205) versus 239 au (95%CI 219-259)). (B) Cumulative distribution plots of the data shown in (A). A KS test showed that the differences between the distributions are not significant ($p = 0.94$).

Fig S16

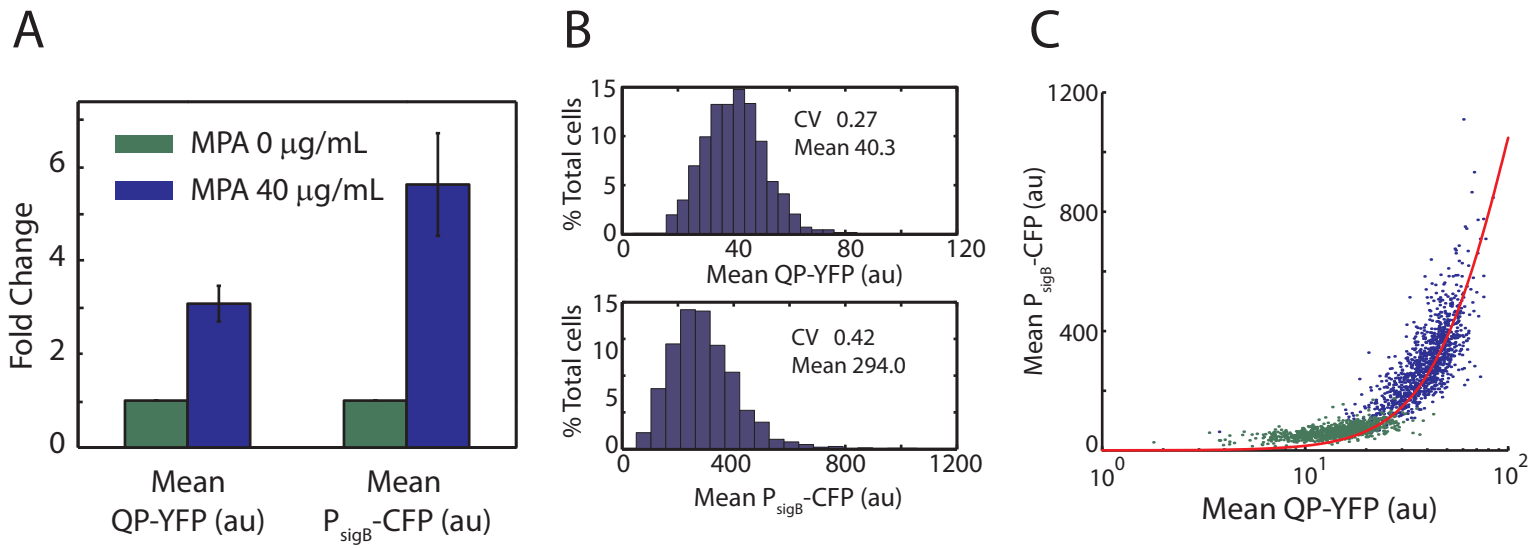

Pulse initiation may result from variability in phosphatase levels. (A) Under energy stress, the fold change in mean σ^B activity is greater than the change in phosphatase QP levels. Strain JJB739 was grown in SMM and exposed to 0 or 40 μg/ml MPA for 180 minutes. The fold change measurement used non-stressed cells (green) as a reference, and was calculated for the stressed condition (blue) using two experiments. Standard error is shown on bar plots. (B) Histograms showing greater variation (measured by CV) of P_{sigB}-CFP (bottom) compared to RsbQP-YFP levels (top). (C) Scatter plot of RsbQP-YFP vs P_{sigB}-CFP from the same data as found in (B). Solid red line represents the hill function fit representing relationship between the overexpression of QP-YFP and P_{sigB}-CFP as found in Fig S11 and Fig 2C). Strong correlation between wild-type RsbQP-YFP and this fit suggests that pulses are initiated by fluctuations in phosphatase levels.

Fig S17

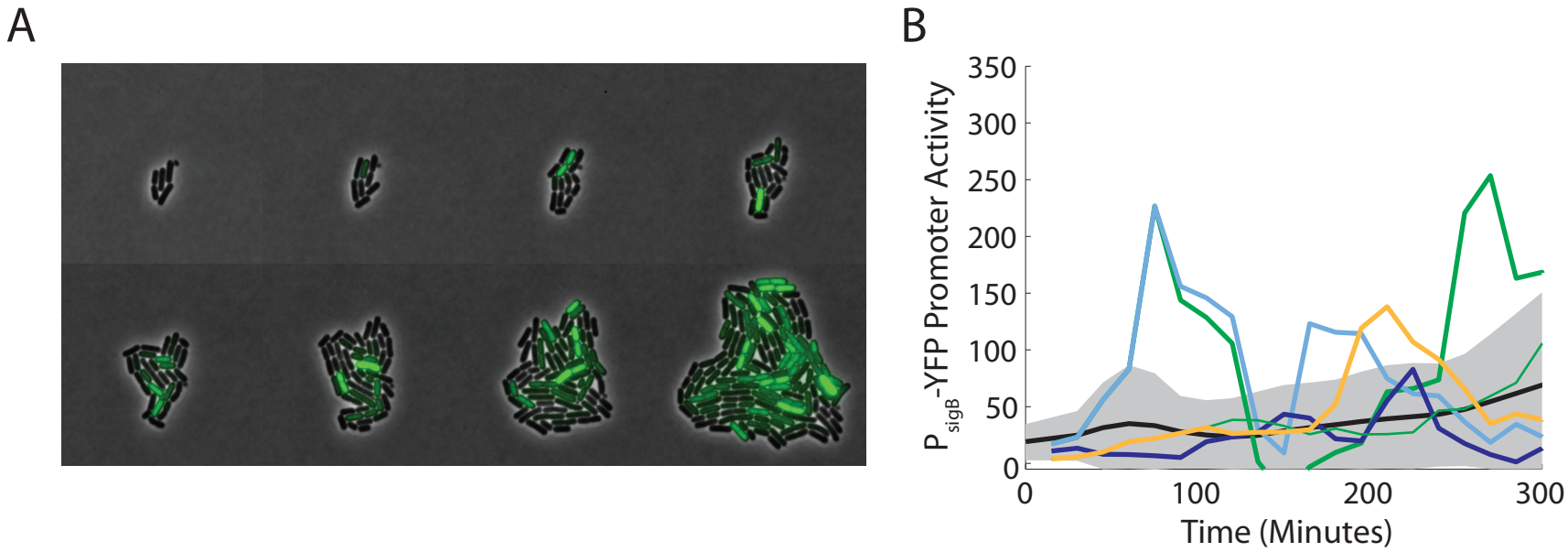

σ^B-YFP pulses can be induced by expression of constitutive phosphatase. A) Film strip of time-lapse movie of P_{sigB}-YFP activity for phosphatase induction strain (JJB643), induced with 7.5 μM IPTG. B) Individual lineage traces (colored lines) showing promoter activity of the P_{sigB}-YFP reporter for phosphatase induction strain. The grey shaded area shows the standard deviation of promoter activity across 2 movies at each timepoint, while the black line is the average promoter activity.

Fig S18

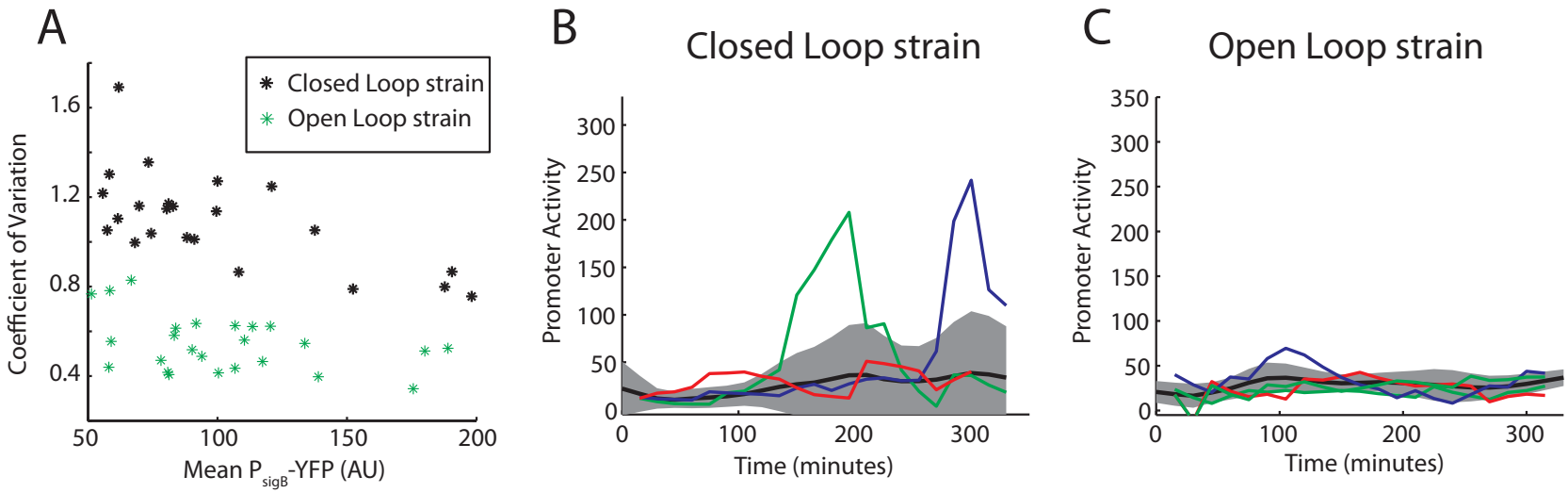

Effects of feedback on pulsing in the rewired input strain. A) Variability in σ^B activity is much reduced in the open loop strain, compared to the closed loop strain. Movies of the open loop strain (strain JJB578) were acquired using the following protocol. First the σ^B operon was induced with 10 μM IPTG, and then 90 min later the phosphatase RsbTU was induced with varying concentrations of xylose (0%, 0.2%, 0.4%, 0.6%, 1.0%, 2.0%),. The mean σ^B level across the entire movie was extracted, and the coefficient of variation (CV) calculated (green stars). Similarly, we computed mean σ^B levels and CV from the closed loop strain movies (black stars, see also Figure 4). The open loop strain (mean CV = 0.5) is much less variable than the closed loop strain (mean CV = 1.1), suggesting a reduction in pulsing. B-C) Individual lineage traces (colored lines) from a closed (B) and open (C) loop strain with the same mean σ^B promoter activity. The grey shaded area shows the standard deviation of promoter activity across each timepoint of the movie, while the black line is the mean promoter activity.

Fig S19

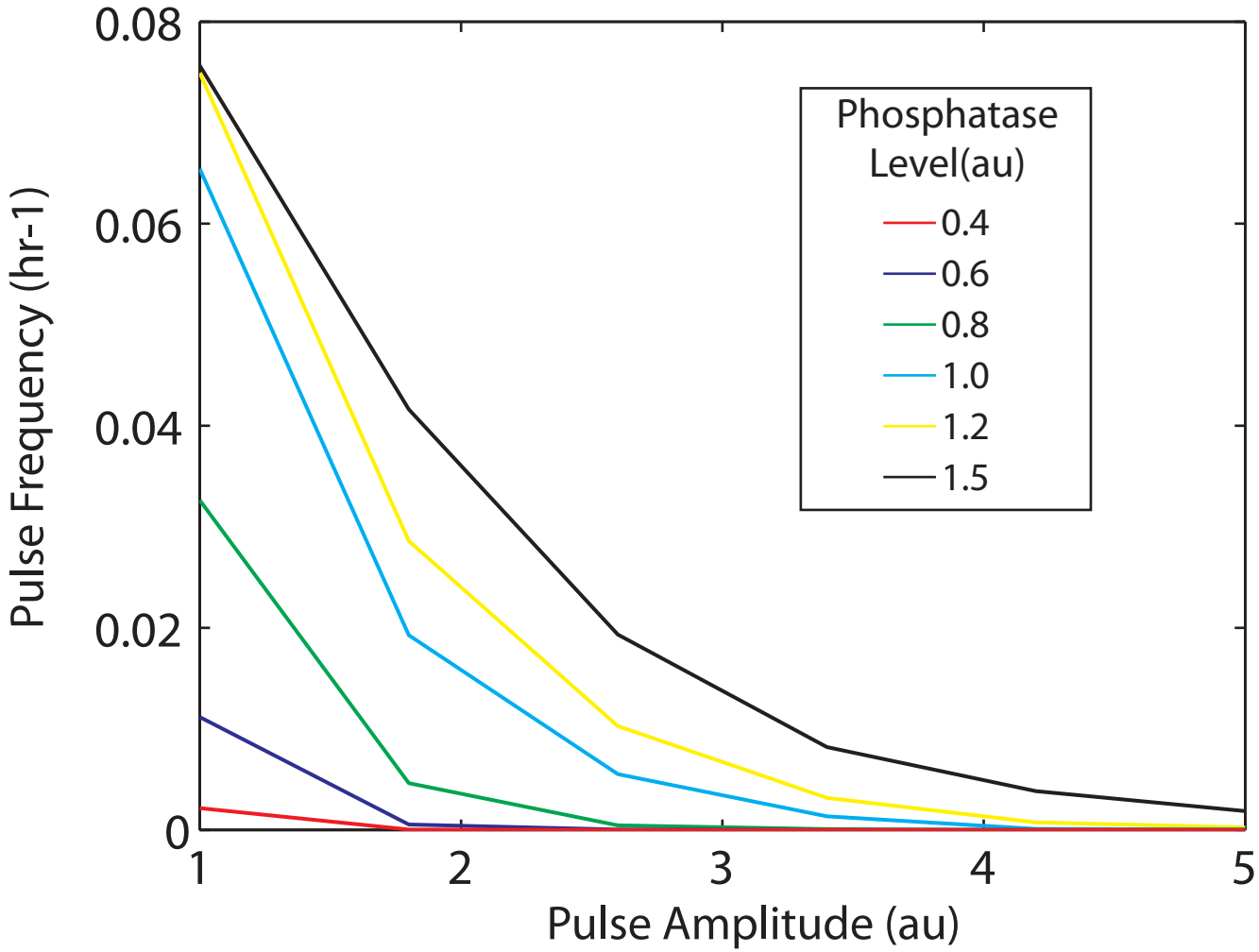

Closed-loop model recapitulates broad pulse amplitude distributions with monotonic decreasing frequency. Pulse statistics were collected from 250 repeats of a 20000 minute numerical simulation , at each phosphatase level. Simulated curves agree with experimental results (compare to figure 1F).

Fig S20

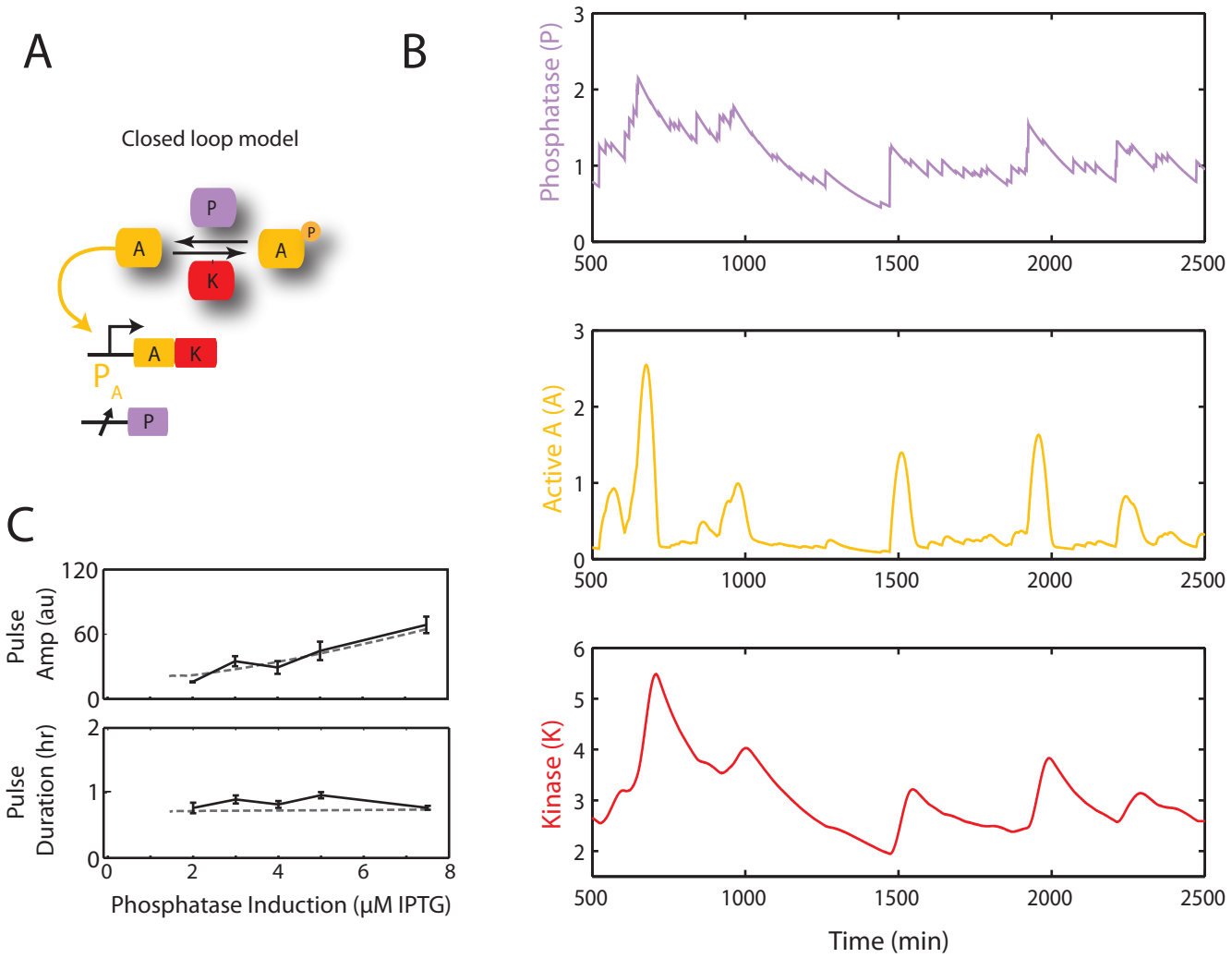

Closed-loop model shows pulsing behavior with noisy phosphatase levels. A minimal closed-loop model of the σ^B system (see supplementary methods), where the inducible phosphatase levels fluctuate through time, gives rise to σ^B pulses and frequency, amplitude, and duration responses that are similar to the closed loop strain (strain JJB643, Fig 4D). (A) Closed-loop model where the output of the system autoregulates the operon. The phosphatase is controlled from an inducible promoter. (B) Simulation results of the closed-loop system. The phosphatase levels (shown in purple) fluctuate according to a gamma distributed Ornstein-Uhlenbeck process, which result in pulses of active A (shown in yellow). Kinase levels (K, red) are upregulated by Active A and shut off pulses. (C) Simulations give rise to pulse characteristics (dashed line) that fit experimental measurements of pulse amplitude and duration (solid black line), as phosphatase is tuned with IPTG (strain JJB643). Due to the small number of pulses at 0 μM IPTG, these data are omitted. For pulse frequency data and simulation, see Fig. 4D. Error bars represent SEM.